



Abstract

The nuclei close to the $N = 101$ show an interesting feature. Distinctly large charge staggering in the isotopic and isomeric shifts was observed for Hg and Tl isotopes, and charge concentration at lower binding energy was observed for Hg, Au, and Pt isotopes. It should also be noted that many high-spin isomers exist in the nuclei of this region, such as Bi, W and Os. For many elements in this region, however, laser spectroscopy

Velocity distribution of ion beams from the RIKEN Ion-Guide Isotope Separator On-Line

Mitsuo Koizumi

Department of Physics, Faculty of Science
Hiroshima University, Higashi-Hiroshima 724, Japan

collinear laser spectroscopy to study exotic nuclei of these elements. To make on-line collinear laser spectroscopy, the radioactive beams from the GARIS/IGISOL is required to have adequate quality (velocity spread, energy spread, etc.). For this, direct measurement of the velocity spread of Au^{197} ion beams from the IGISOL was carried out with a technique of laser spectroscopy. The dependence of the velocity spread on the extraction voltage was introduced to reduce the velocity spread, and the effect of this was experimentally examined. From these measurements, it was pointed out that the ion beam from the GARIS/IGISOL has adequate quality for making collinear laser spectroscopy. An estimation of the yield of radioactive isotope from the GARIS/IGISOL was also made for a fusion reaction $^4\text{He} + ^{100}\text{Br} \rightarrow ^{104}\text{Kr}$. The estimated yield was expected to be more than 10^4 particles/s. The yield of the radioactive isotope is adequate for making collinear laser spectroscopy with X-ray detector system. We have for the first time in the world extracted the radioactive isotope of secondary element ^{104}Kr with the GARIS/IGISOL. We conclude, thus, that the collinear laser spectroscopy of refractory elements with the GARIS/IGISOL is promising.

Abstract

The nuclei close to the $N = 104$ show an interesting feature. Extremely large shape staggering in the isotope and isomer shifts was observed for Hg and Tl isotopes, and shape coexistence at low excitation energy was observed for Hg, Au, and Pt isotopes. It should also be noted that many high-spin isomers exist in the nuclei of this region, such as Hf, W and Os. For many elements in this region, however, laser spectroscopy has not been reported, because these elements are refractory ones. At RIKEN, we have constructed an ISOL system GARIS/IGISOL which is powerful to extract radioactive isotopes of refractory elements. Taking full advantages of this feature, we aim at performing collinear laser spectroscopy to study exotic nuclei of these elements. To make on-line collinear laser spectroscopy, the radioactive beams from the GARIS/IGISOL is required to have adequate quality (velocity spread) and quantity. Therefore, direct measurement of the velocity spread of Ar^{1+} ion beams from the IGISOL was carried out with a technique of laser spectroscopy. The skimmer-potential and the gas-cell pressure dependences of the velocity spread were systematically investigated. A new focusing device SQUEEZER was introduced to reduce the velocity spread, and the effect of this was experimentally examined. From these measurements, it was pointed out that the ion beam from the GARIS/IGISOL has adequate quality for making collinear laser spectroscopy. An estimation of the yield of radioactive isotopes from the GARIS/IGISOL was also made for a fusion reaction ${}^9\text{Be}({}^{166}\text{Er}, xn){}^{175-x}\text{Hf}$. The estimated yield was expected to be more than 10^4 particles/s. The yield of the radioactive isotope is adequate to make collinear laser spectroscopy with a coincidence method. We have for the first time in the world extracted the radioactive isotope of refractory element ${}^{169}\text{Hf}$ with the GARIS/IGISOL. We conclude, thus, that the collinear laser spectroscopy of refractory elements with the GARIS/IGISOL is promising.

Contents

1	Introduction	1
2	Principle of measurement	5
2.1	Doppler shift and Doppler broadening	5
2.2	Mass resolving power (MRP)	8
3	Experimental	11
3.1	Location of IGISOL	11
3.2	SQUEEZER	11
3.3	Discharge ion source	14
3.4	Laser system	18
3.5	Experimental setup for velocity measurement	18
3.6	Production of radioactive isotope of a refractory element: ^{169}Hf	22
4	Results and discussion	24
4.1	LIF spectrum of Ar^{1+}	24
4.2	Velocity spread and beam divergence	24
4.3	Skimmer-voltage dependence of the velocity spread	27
4.4	The effect of SQUEEZER	28
4.5	He-gas pressure dependence of the velocity spread	29
4.6	Comparison with the mass resolving power	30
4.7	Velocity distribution of a collimated beam	35
4.8	Mass dependence of the MRP	35

4.9	Yield of radioactive isotopes from the GARIS/IGISOL	37
4.10	Feasibility of on-line collinear laser spectroscopy	38
5	Conclusion	41
	Appendix	43
A	Collinear laser spectroscopy setup for on-line experiment	43
B	High-resolution off-line laser spectroscopy setup for refractory elements . .	48
	Acknowledgment	52
	References	53

The accessible area on the chart of the nuclides is extending further and further away from the β -stability line with development of an accelerator and an isotope separator on-line (ISOL). To study the basic properties of exotic nuclei, the method of laser spectroscopy was combined with the ISOL technique [6, 7]. For many elements, valuable knowledge of the nuclear structure have been obtained systematically for many long isotopic chains [6, 7, 8].

For the mercury nuclei close to $N = 104$, extremely large odd-even staggering in the isotope and isomer shifts has been observed [9]. This staggering is understood as a change of the nuclear shape, i.e., oblate-prolate shape staggering [8]. This staggering was quite an unexpected feature for nuclei very close to the spherical closed-shell $Z = 82$. Following this discovery, the coexistence of different shapes, well-deformed and near-spherical, was observed for mercury isotopes by means of systematic in-beam γ spectroscopy [9]. It is also surprising that the nuclei have second minima of their potential energy surfaces at low spins and low excitation energy, and the potential barrier between the first (ground

1 Introduction

The existence of atomic nuclei is reflected in the atomic energy levels through a small but well-defined electromagnetic interaction [1, 2]. The precise study of the atomic spectra, therefore, provides fundamental information on nuclear ground-state and isomeric-state properties without using any nuclear model: changes of mean-square nuclear charge radii ($\delta \langle r^2 \rangle$) are deduced from isotope shifts; nuclear spins (I) and nuclear electromagnetic moments (μ , Q , ...) are deduced from hyperfine structures. High-resolution laser spectroscopy has successfully been made to study these nuclear properties [3, 4, 5].

The accessible area on the chart of the nuclides is extending further and further away from the β -stability line with development of an accelerator and an isotope separator on-line (ISOL). To study the basic properties of exotic nuclei, the method of laser spectroscopy was combined with the ISOL technique [6, 7]. For many elements, valuable knowledges of the nuclear structure have been obtained systematically for many long isotopic chains [6, 7, 8].

For the mercury nuclei close to $N = 104$, extremely large odd-even staggering in the isotope and isomer shifts has been observed [8]. This staggering is understood as a change of the nuclear shape, i.e., oblate-prolate shape staggering [8]. This staggering was quite an unexpected feature for nuclei very near to the spherical closed-shell $Z = 82$. Following this discovery, the coexistence of different shapes, well-deformed and near-spherical, was observed for mercury isotopes by means of systematic in-beam γ spectroscopy [9]. It is also surprising that the nuclei have second minima of their potential-energy surfaces at low spin and low excitation energy, and the potential barrier between the first (ground

state) and second minima is high enough to build complete bands. For Au and Pt isotopes, the shape coexistence was also observed [10]. In this region, the potential-energy surface of nuclei changes drastically as a function of neutron and proton numbers. Therefore, it is interesting to study the nuclear shapes systematically in such a transitional region. Moreover, it should be pointed out that high-spin isomers exist in the transitional region, for instance, in nuclei of Hf, W, and Os. It is also interesting to know the shapes of high-spin isomers, because there are two possibilities to generate such high-spins: One is the alignment of a few nucleons along the symmetry axis and the other is collective motion. The former is called high-K isomer and the latter shape isomer.

Laser spectroscopy is suitable to study nuclear shapes of ground and isomeric states systematically. For Tl, Au and Pt elements, isotope- and isomer-shift measurements have already started [11, 12, 13]. For refractory elements such as Hf, W, and Os, however, on-line collinear laser spectroscopy has never been reported, because it is hard to extract these elements from a conventional isotope separator equipped with a heated-ion source [14].

An ISOL system, which consists of a gas-filled recoil isotope separator (GARIS) and an ion-guide isotope separator on-line (IGISOL), has been constructed being combined in tandem at RIKEN Accelerator Research Facility [15, 16]. This system has no heated-ion source, so that it provides us great possibility to study the nuclei of refractory elements on-line.

The IGISOL was first developed at the University of Jyväskylä [17]. With this system, they actually showed that short-lived isotopes of the order of one millisecond half-life could be extracted even though they are refractory elements [18]. Therefore, the

system GARIS/IGISOL is considered an extremely powerful tool in separating refractory elements. In fact, a radioactive isotope of refractory element, ^{169}Hf , has been extracted from this system [19]. We now aim at performing collinear laser spectroscopy to study radioactive isotopes of refractory elements with the GARIS/IGISOL.

On the other hand, the mass resolving power (MRP) of an IGISOL was reported to be lower than that of the conventional ISOL. The energy spread of the IGISOL ion beam deduced from the MRP was more than 100 eV [20, 21, 22]. For the conventional ISOL, the energy spread is less than 10 eV [14], where collinear laser spectroscopy has been established. This suggests that the ion beam from the IGISOL is inadequate to do collinear laser spectroscopy. It should be pointed out, however, that the estimation of the energy spread of the IGISOL ion beam was made on the assumption that the MRP depends only on the momentum spread of the ion beam. To discuss the feasibility of laser spectroscopy using the GARIS/IGISOL, it is important to measure directly the velocity spread of ion beams from the IGISOL.

Laser spectroscopy is ideally suited for measuring the velocity and its distribution of an atomic beam, because the resonance spectrum reflects the beam quality along the direction of the laser beam as the Doppler shift and broadening. From a measurement at collinear geometry, the longitudinal velocity and its distribution are deduced, and from a measurement at 90° incidence, the transversal velocity distribution or beam divergence is deduced. In principle, this method is applicable to various elements in the form of atoms, ions and molecules.

At a relatively low acceleration potential, direct measurement of the velocity distribution of an Ar^{1+} ion beam by means of collinear laser spectroscopy was performed

by N. Schmidt at Mainz university [23]. In the light of his experiment, we have measured the velocity distribution of the Ar^{1+} ion beam from the IGISOL for the first time. It was pointed out that the MRP depends on the skimmer potential and pressure in the gas cell [20, 21, 22]. Therefore, we measured the velocity distribution of the ion beam from the IGISOL systematically, changing the condition of the IGISOL.

It is also important to produce an adequate number of radioactive isotopes for collinear laser spectroscopy, because a beam intensity of more than 10^4 particles/s is required [7]. The efficiency of the GARIS/IGISOL has been experimentally determined [16]. According to the previous results [16], the estimation of the yield of radioactive isotope from the GARIS/IGISOL has been made, and the production of the unstable nuclei ^{169}Hf has been experimentally done.

In this paper, we shall present the results of our velocity spread measurement, and discuss how to obtain the ion beam with a narrow energy spread. We shall also show the estimated and experimentally obtained yield of radioactive isotopes from the GARIS/IGISOL. Finally, the feasibility of laser spectroscopy with the GARIS/IGISOL will be discussed in detail.

2 Principle of measurement

2.1 Doppler shift and Doppler broadening

Laser spectroscopy is a powerful method to measure the velocity distribution of atomic beams. The Doppler shift and broadening are the reflection of the velocity of the atomic beam and its spread along the direction of the laser beam. The relation between the resonance frequencies of the atom in the rest frame (ν_0) and in the laboratory frame (ν) is given by

$$\begin{aligned}\nu &= \nu_0 \frac{\sqrt{1 - \beta^2}}{1 - \beta \cos \theta} \\ &= \nu_0 \left(1 + \beta \cos \theta - \frac{1}{2}\beta^2 + \beta^2 \cos^2 \theta \dots \right),\end{aligned}\quad (1)$$

where θ is the incident angle between laser and ion beams, and $\beta = v/c$. (See fig. 1.) The velocity of the atom is given by v and c is the velocity of light. The Doppler shift ν_D is then written as

$$\nu_D = \nu_0 \left(\beta \cos \theta - \frac{1}{2}\beta^2 + \beta^2 \cos^2 \theta \dots \right). \quad (2)$$

The Doppler broadening $\Delta\nu_D$ is caused by the velocity distribution $\pm\delta\beta$ and the angular dispersion $\pm\delta\theta$. Here we define the sign Δ as the full width at half maximum (FWHM) of any distribution and the sign δ as the half width at half maximum (HWHM). The quantities $\delta\beta$ and $\delta\theta$ can be treated independently, so that we have

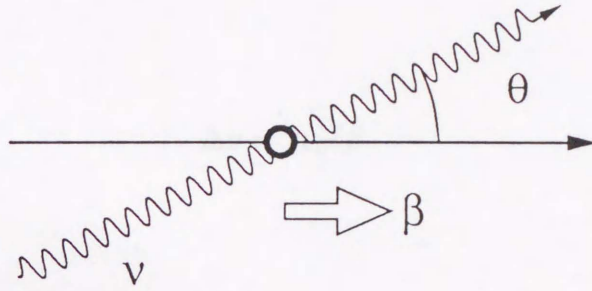


Figure 1: The relation between the laser and ion beams.

$$(\Delta\nu_D)^2 = (\Delta\nu_\beta)^2 + (\Delta\nu_\theta)^2, \quad (3)$$

where $\Delta\nu_\beta$ is a Doppler spread due to the velocity distribution and $\Delta\nu_\theta$ is the one due to the dispersion of the ion and laser beams.

To first order of β , the Doppler shift is given by

$$\nu_D = \nu_0(\beta \cos \theta). \quad (4)$$

The contributions to the broadening is then written as

$$\begin{aligned} \Delta\nu_\beta &= 2\nu_0\delta\beta \cos \theta, \\ \Delta\nu_\theta &= 2\nu_0\beta\delta\theta \sin \theta. \end{aligned} \quad (5)$$

For a collinear geometry (180° incidence), $\Delta\nu_\theta = 0$, and we obtain the Doppler broadening

$$\Delta\nu = 2\nu_0\delta\beta. \quad (6)$$

For 90° incidence, $\Delta\nu_\beta = 0$, and we obtain

$$\Delta\nu = 2\nu_0\beta\delta\theta. \quad (7)$$

As shown in eqs. (6) and (7), the velocity distribution can be deduced from a collinear measurement, and the angular distribution from a measurement at 90° incidence.

To second order of β , the Doppler shift is given by

$$\nu_D = \nu_0 \left(\beta \cos \theta - \frac{1}{2}\beta^2 + \beta^2 \cos^2 \theta \right). \quad (8)$$

Contributions to the Doppler broadening are given by, to second order of $\delta\beta$ and $\delta\theta$,

$$\begin{aligned} \Delta\nu_\beta &= 2\nu_0 \left(\delta\beta \cos \theta - \beta\delta\beta + 2\beta\delta\beta \cos^2 \theta - \frac{1}{2}\delta\beta^2 + \delta\beta^2 \cos^2 \theta \right), \\ \Delta\nu_\theta &= 2\nu_0 \left(\beta\delta\theta \sin \theta + 2\beta^2\delta\theta \cos \theta \sin \theta \right. \\ &\quad \left. + \frac{1}{2}\beta\delta\theta^2 \cos \theta + \beta^2\delta\theta^2 (1 - 2\sin^2 \theta) \right). \end{aligned} \quad (9)$$

The velocity is so small that the kinetic energy E is safely given by the non-relativistic expression

$$E = eU = \frac{1}{2}mc^2\beta^2. \quad (10)$$

The energy spread ΔE is therefore

$$\Delta E = mc^2\beta\Delta\beta, \quad (11)$$

and we have

$$\frac{\Delta E}{E} = \frac{\Delta U}{U} = 2\frac{\Delta\beta}{\beta}. \quad (12)$$

For collinear measurement we have, to first order of β ,

$$\frac{\Delta E}{E} = \frac{\Delta U}{U} = 2\frac{\Delta\nu}{\nu_D}. \quad (13)$$

2.2 Mass resolving power (MRP)

The relation of the magnetic field B of an analyzing magnet and an analyzed ion beam with mass M and a kinetic energy E was given by

$$qB\rho = P = \sqrt{2ME}, \quad (14)$$

where ρ is a radius of the central ray of the analyzing magnet and q charge of the ion. The ΔB of mass spectrum corresponding to the ΔM as shown in fig. 2 is, therefore, written as

$$\Delta B = \frac{1}{2} \frac{1}{q\rho} \sqrt{2E} \frac{\Delta M}{\sqrt{M}}. \quad (15)$$

The value ΔM is a reduced value from the energy spread ΔE . Therefore the relationship between the MRP and the energy broadening is

$$MRP = \frac{M}{\Delta M} = \left(\frac{E}{\Delta E} \right)_M = \left(\frac{U}{\Delta U} \right)_M. \quad (16)$$

Here, we should bear in mind that this relation is valid only for ideal beam optics, i.e., no emittance is taken into account.

3 Experimental

3.1 Location of IGISOL

The RIKEN ISOL system, which consists of the GARIS and the IGISOL, is shown in Fig. 3 [15, 16]. The GARIS has three magnets arranged in a D-Q-Q configuration, and the IGISOL is connected in tandem with the GARIS. The components of the IGISOL are an injection chamber, an accelerating section, a beam transport section, a magnetic separator, an electrostatic mass analyzer and three beam lines. The 45° and 25° beam lines are designed for point-to-parallel and parallel-to-parallel beam transport, respectively. The configuration of the ion-guide chamber is shown in Fig. 4. The purpose of the GARIS is to separate most products from the incident beam and to provide the beam with a velocity spread in the gas cell. In order to avoid a plasma effect first seen in the GARIS, the transport of the beam is done in the gas cell. The beam is then transported with an energy degrader and a helium buffer gas. The stopped radioactive

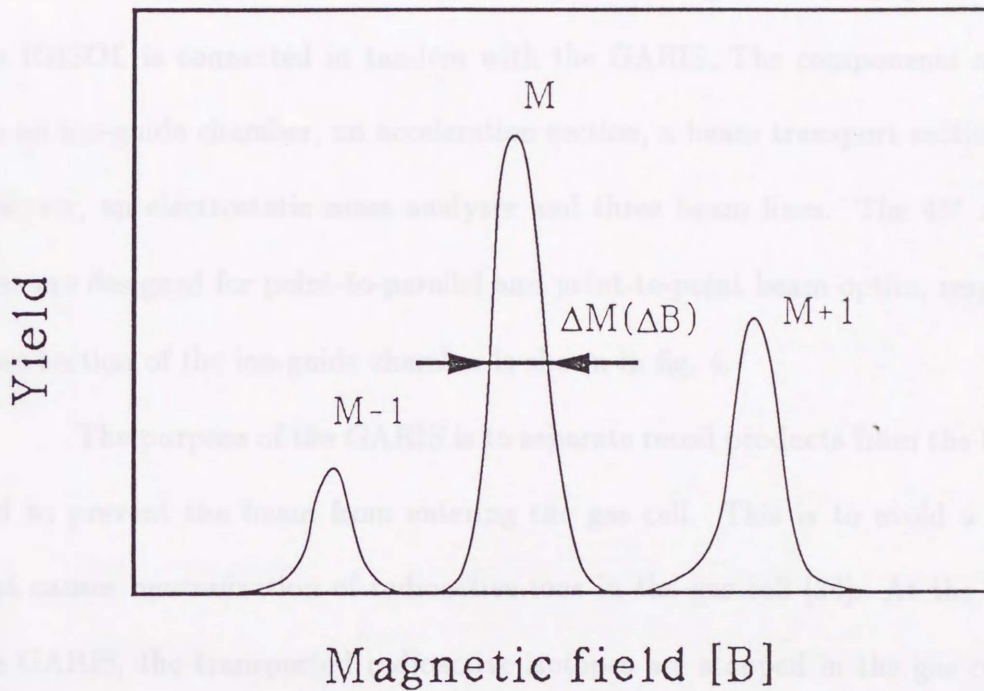


Figure 2: A mass spectrum observed as a function of magnetic field B of the analyzing magnet. The value of ΔM is a FWHM of the mass spectrum associated with ΔB .

3.2 SQUEEZER

It is known that higher MRP is obtained for the lower skimmer potential [22]. However, the yield of the radioactive isotope extracted from the IGISOL decreases for the lower skimmer potential [22]. To obtain high MRP without losing the efficiency of IGISOL, a group of Jyväskylä developed a new focusing device SQUEEZER [26]. The SQUEEZER

3 Experimental

3.1 Location of IGISOL

The RIKEN ISOL system, which consists of the GARIS and the IGISOL, is shown in fig. 3 [15, 16]. The GARIS has three magnets arranged in a D-Q-Q configuration, and the IGISOL is connected in tandem with the GARIS. The components of the IGISOL are an ion-guide chamber, an acceleration section, a beam transport section, a magnetic analyzer, an electrostatic mass analyzer and three beam lines. The 45° and 90° beam lines are designed for point-to-parallel and point-to-point beam optics, respectively. The cross-section of the ion-guide chamber is shown in fig. 4.

The purpose of the GARIS is to separate recoil products from the incident beam and to prevent the beam from entering the gas cell. This is to avoid a plasma effect that causes neutralization of radioactive ions in the gas cell [24]. At the focal point of the GARIS, the transported radioactive isotopes are stopped in the gas cell of the ion-guide chamber with an energy degrader and a helium buffer gas. The stopped radioactive products are cooled down and thermalized by collisions with helium atoms. A part of the products survives as singly charged ions in the gas cell. They are guided by a helium gas flow to the skimmer and thus extracted by electric fields of the skimmer and the extractor.

3.2 SQUEEZER

It is known that higher MRP is obtained for the lower skimmer potential [22]. However, the yield of the radioactive isotope extracted from the IGISOL decreases for the lower skimmer potential [22]. To obtain high MRP without losing the efficiency of IGISOL, a group of Jyväskylä developed a new focusing device SQUEEZER [25]. The SQUEEZER

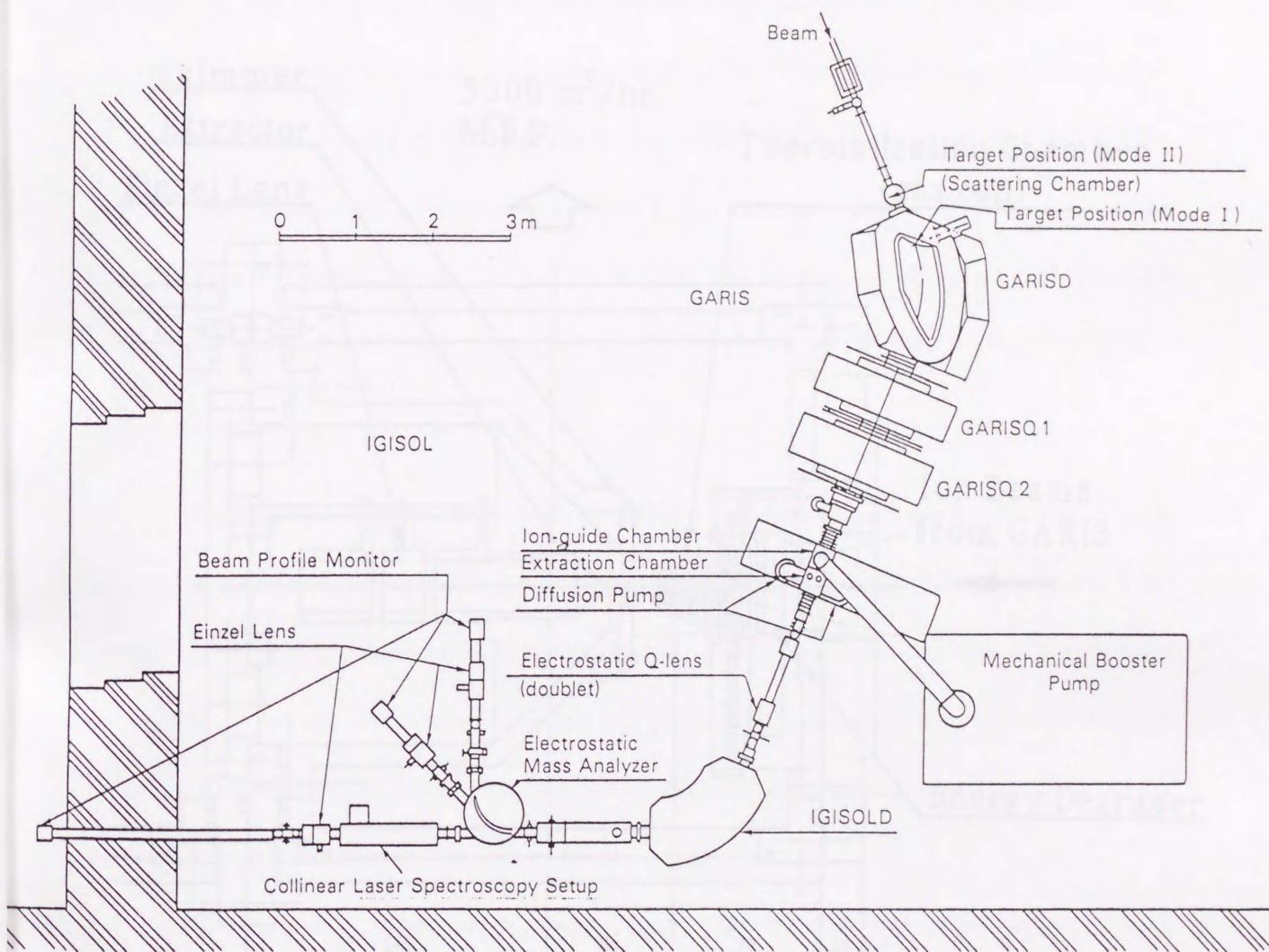


Figure 3: A layout of the RIKEN ISOL, GARIS/IGISOL.

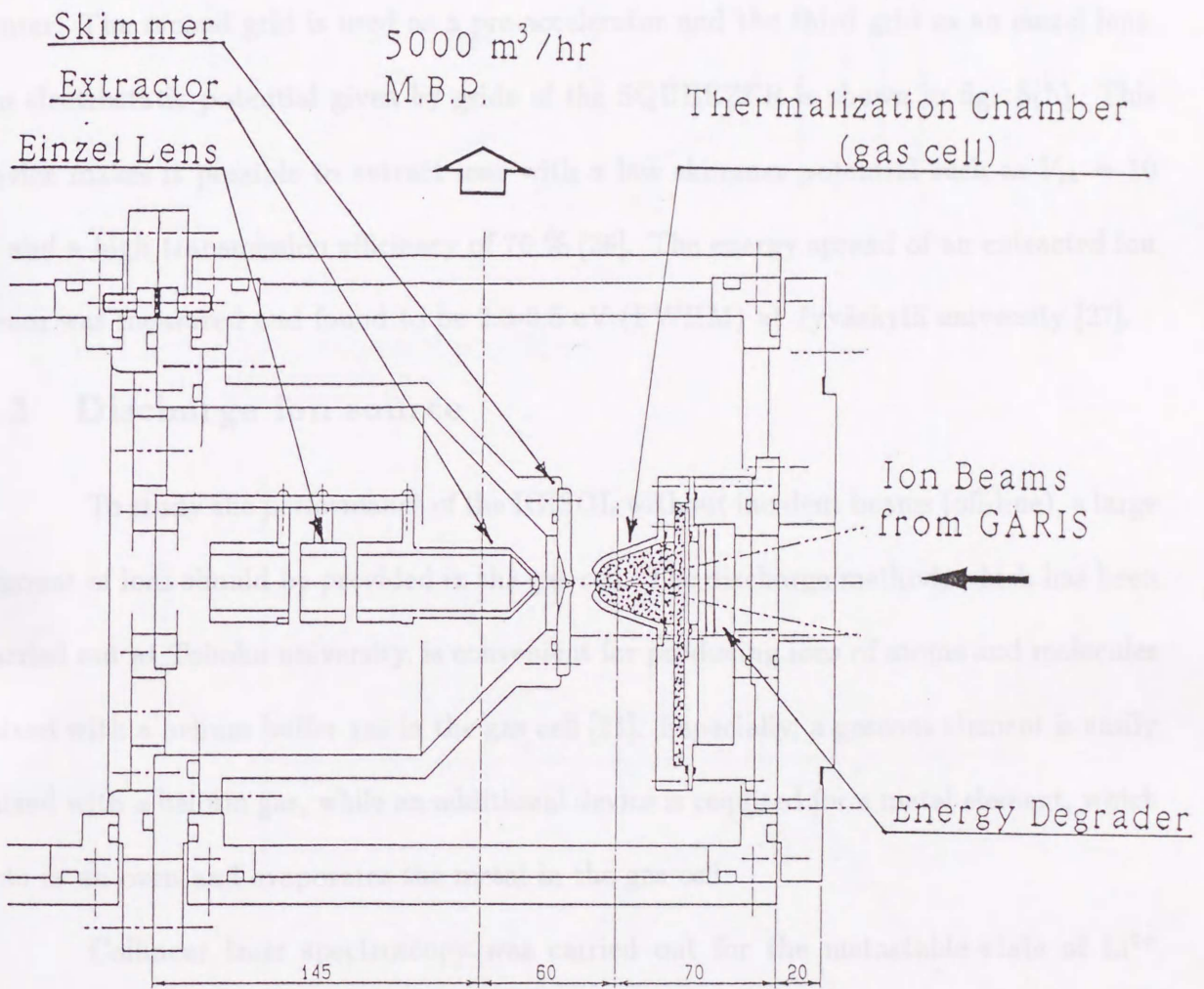


Figure 4: An ion-guide chamber housing a gas cell with an energy degrader, a skimmer, an extractor and an einzel lens.

is set between the gas cell and skimmer as shown in fig. 5(a). The SQUEEZER has three grids. To the first grid, a low positive potential is supplied. The positive ions coming from the exit hole of the gas cell are pushed by the helium gas flow and climb the potential hill produced by the first grid. In this process, the ion beam slows down and is focused to the center. The second grid is used as a pre-accelerator and the third grid as an einzel lens. An electrostatic potential given by grids of the SQUEEZER is shown in fig. 5(b). This device makes it possible to extract ions with a low skimmer potential such as $V_{sk} = 10$ V and a high transmission efficiency of 70 % [26]. The energy spread of an extracted ion beam was measured and found to be 2.3-3.5 eV (FWHM) at Jyväskylä university [27].

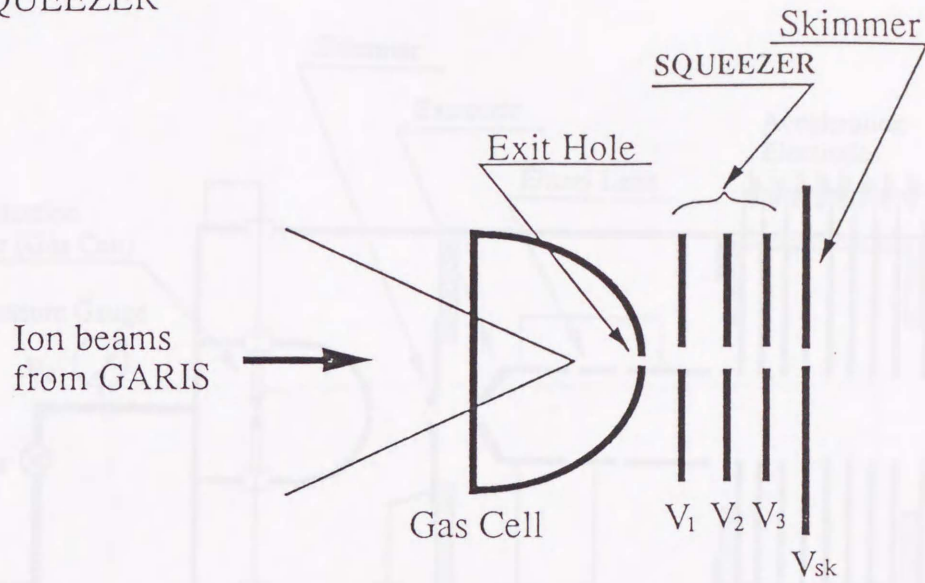
3.3 Discharge ion source

To study the performance of the IGISOL without incident beams (off-line), a large amount of ions should be provided in the gas cell. The discharge method, which has been carried out at Tohoku university, is convenient for producing ions of atoms and molecules mixed with a helium buffer gas in the gas cell [21]. Especially, a gaseous element is easily mixed with a helium gas, while an additional device is required for a metal element, which acts as an oven and evaporates the metal in the gas cell.

Collinear laser spectroscopy was carried out for the metastable state of Li^{1+} and Ar^{1+} by N. Schmidt at Mainz university [23]. For our velocity measurement, laser spectroscopy of ions (not neutral atoms) is suitable because there is no need to neutralize ion beam using a charge exchange cell. And it is much easier to handle gaseous Ar than to handle active Li as mentioned above. Therefore in the light of the Schmidt's experiment [23], we have measured the velocity spread of Ar^{1+} ion beam from the IGISOL.

The schematic diagram of the ion-guide chamber housing discharge electrodes is

(a) SQUEEZER



(b) Electrostatic potential produced by the SQUEEZER

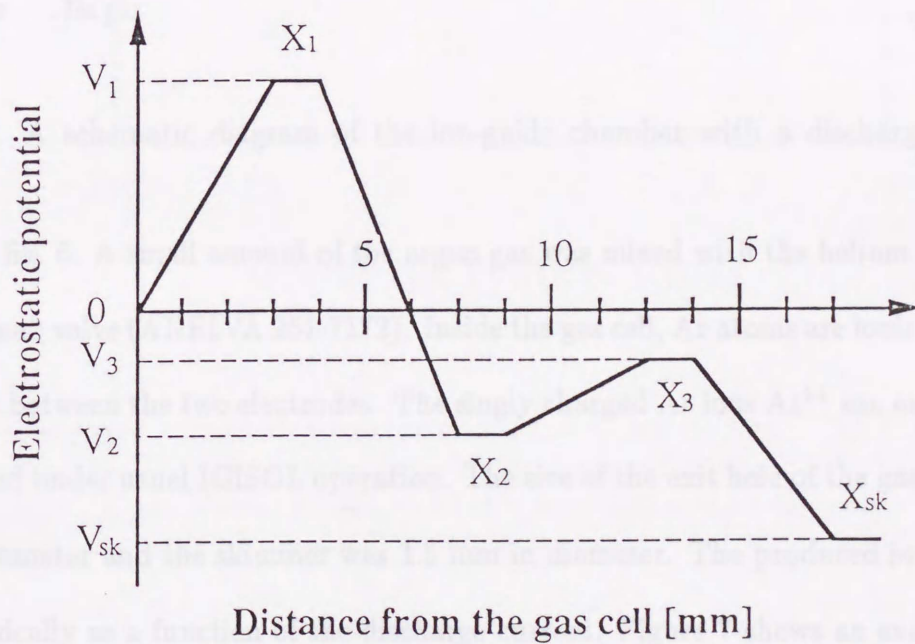


Figure 5: (a) Schematic diagram of SQUEEZER set in the ion-guide chamber. (b) Electrostatic potential associated with the SQUEEZER. The potential of the gas cell is taken as 0 V. The abscissa is a distance from the exit hole of the gas cell. The positions of grids of the SQUEEZER and the skimmer are given by X_1 , X_2 , X_3 , and X_{sk} , respectively.

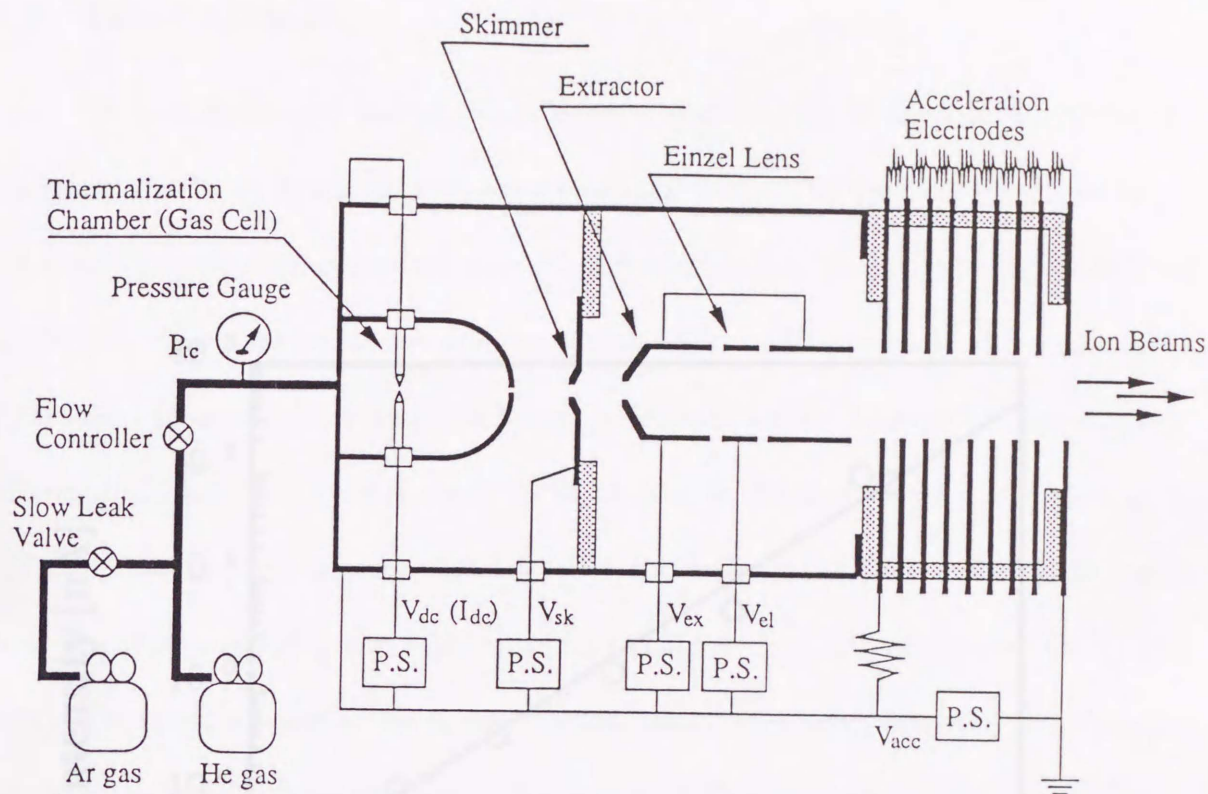


Figure 6: A schematic diagram of the ion-guide chamber with a discharge ionization device.

shown in fig. 6. A small amount of the argon gas was mixed with the helium gas through the slow leak valve (ANELVA 951-7172). Inside the gas cell, Ar atoms are ionized by a glow discharge between the two electrodes. The singly charged Ar ions Ar^{1+} are extracted and accelerated under usual IGISOL operation. The size of the exit hole of the gas cell was 1.1 mm in diameter and the skimmer was 1.5 mm in diameter. The produced ions increased logarithmically as a function of the discharge current. Figure 7 shows an example of the performance of the discharge ion source.

3.4 Laser system

A laser beam used was produced by a cw He-Ne laser (Coherent SP-20), which was pumped with an Ar ion laser (Spectra Physics 171-10). The dye used was Rhodamine 6G, which is applicable to produce a laser beam varying in a wavelength range of 590 nm

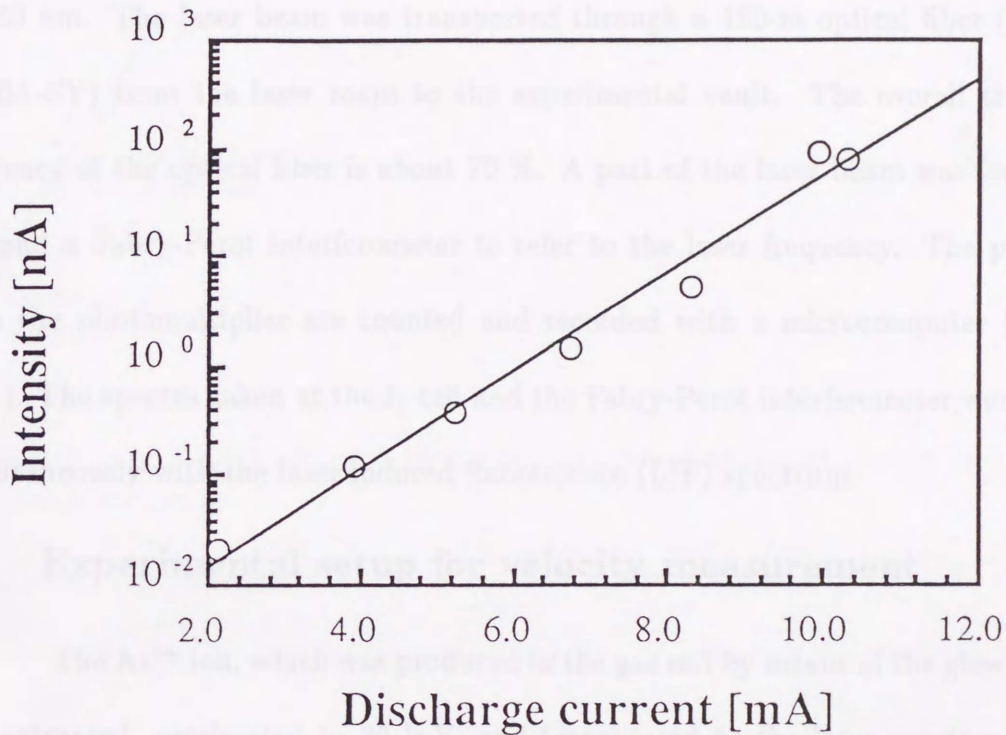


Figure 7: Discharge current dependence of the ion beam current. The beam current extracted from the IGISOL increases logarithmically as a function of discharge current. The pressure in the gas cell was 20 mbar, and the potentials at electrodes were $V_{sk} = -500$ V, $V_{ex} = 10$ kV, $V_{el} = 5.7$ kV, and $V_{acc} = 30$ kV.

3.4 Laser system

A laser beam used was produced by a cw ring dye laser (Coherent 699-29), which was pumped with an Ar ion laser (Spectra Physics 171-19). The dye used was Rhodamine-6G, which is applicable to produce a laser beam varying in a wavelength range of 550 nm \sim 650 nm. The laser beam was transported through a 160-m optical fiber (Mitsubishi ST50A-SY) from the laser room to the experimental vault. The overall transmission efficiency of the optical fiber is about 70 %. A part of the laser beam was sent to an I₂ cell and a Fabry-Perot interferometer to refer to the laser frequency. The pulse signal from the photomultiplier are counted and recorded with a microcomputer (NEC PC-9801). The spectra taken at the I₂ cell and the Fabry-Perot interferometer were recorded simultaneously with the laser induced fluorescence (LIF) spectrum.

3.5 Experimental setup for velocity measurement

The Ar¹⁺ ion, which was produced in the gas cell by means of the glow discharge, was extracted, accelerated to 30 keV, and transported to the laser spectroscopy setup as schematically shown in fig. 8. At the focal point of the analyzing magnet, we have a mass defining slit and a Faraday-cup, which are used for mass-spectrum measurement. The mass-separated ion beam was deflected by an electrostatic mass analyzer. The LIF observation section was set on the 45° beam line, which is designed for point-to-parallel beam optics. An electrostatic quadrupole doublet and an einzel lens were used as a focusing element. At the LIF observation section, the ion beam intersected the laser beam at the angle of 30°, 90°, and 180°. The size of the ion beam at the interaction region was about 0.5 cm in diameter, and the size of the laser beam about 1 cm in

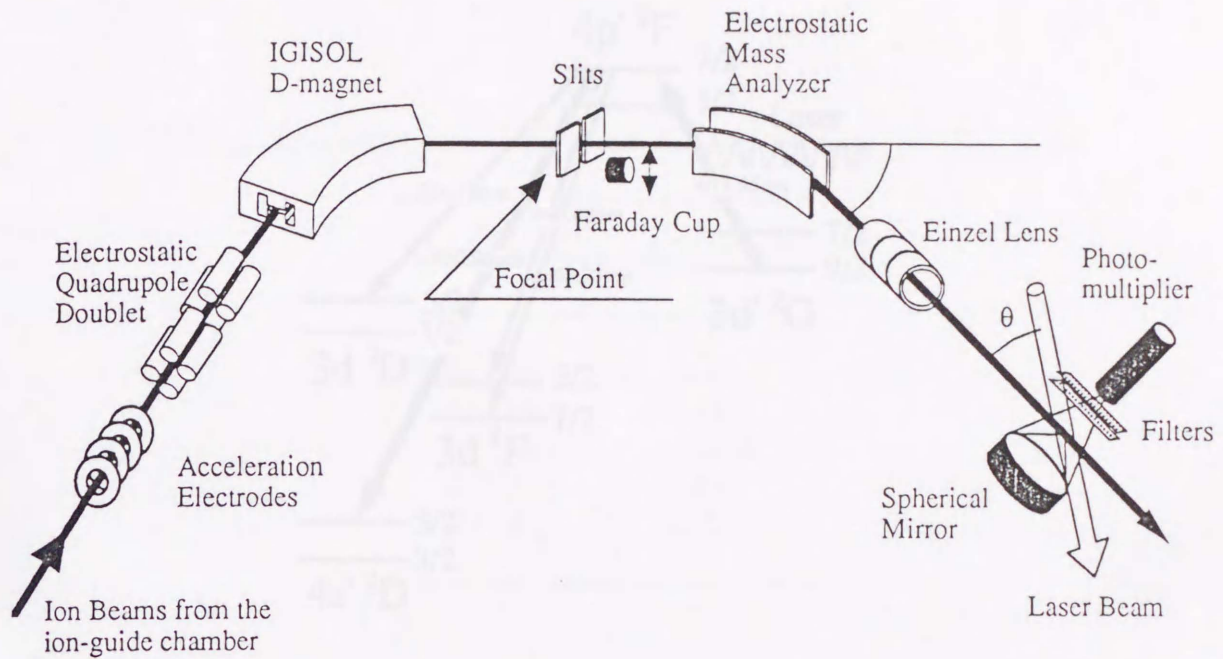


Figure 8: A schematic diagram of the IGISOL beam transport system and the LIF observation section.

diameter. The laser power at the interaction region was typically 100 mW.

The 611.66-nm transition from the $3d' \ ^2G_{9/2}$ metastable state to the $4p' \ ^2F_{7/2}$ state in Ar^{1+} was observed. The resonance wavelength of the laser beam for collinear geometry (180° incidence), for example, is 612.44 nm at $U = 30$ kV and the Doppler shift of the resonance frequency is 622 GHz. The atomic energy levels of Ar^{1+} associated with the measurement are shown in fig. 9. Fluorescence photons emitted from the $4p' \ ^2F_{7/2}$ level was collected with a spherical mirror, which was 80 mm in diameter and 60 mm in radius of curvature. The solid angle of photon collection is 0.95π sr. The background photons are mainly stray lights from the laser beam and scattered lights from ions, which is produced by the collision with residual gas during the flight in the vacuum chamber. Because of the large difference between the wavelength of the laser beam and fluorescence

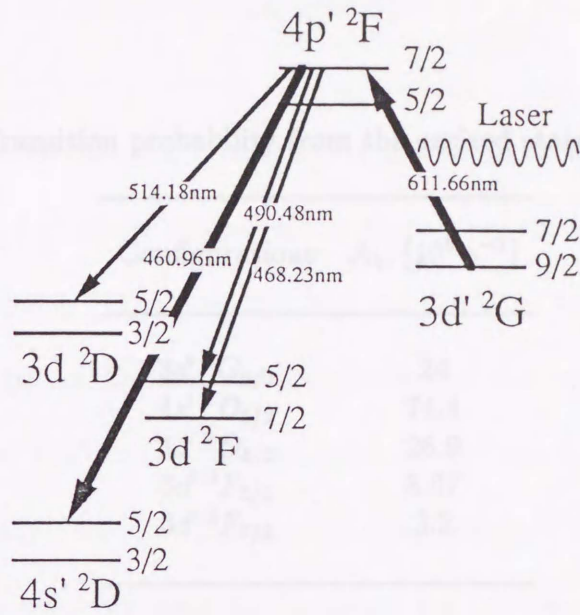


Figure 9: Atomic energy levels of Ar^{1+} associated with the measurement.

lights, a band pass filter effectively reduces the background photons. The 460.96-nm transition from the excited state $4p' \ ^2F_{7/2}$ to the state $4s' \ ^2D_{5/2}$ was selectively observed because this transition is strongest [23]. (See table 1.) The band pass filters used were Shott BG25 and Kenko BP-46, which were set just in front of the single-photon counting photomultiplier (Hamamatsu R329-02).

For collinear geometry, the population of the ions in the metastable state rapidly decreases during the flight in the resonance laser field because of optical pumping: the ions in the metastable state are repeatedly excited by the resonance laser field and decay to other levels. Therefore an additional acceleration electrode was set at the observing section as shown in fig 10. This device prevents the optical pumping by changing the ion velocity, i.e., the resonance frequency of moving atoms. Here we applied negative voltage of 100 V to the electrode.

3.6 Production of radioactive isotope of a refractory element ^{109}Rh

Table 1: Transition probability from the excited state $4p' \ ^2F_{7/2}$ [23].

Configurations	A_{ki} [10^6 s^{-1}]
$3d' \ ^2G_{9/2}$	24
$4s' \ ^2D_{5/2}$	74.4
$3d' \ ^2D_{5/2}$	26.9
$3d' \ ^2F_{5/2}$	8.07
$3d' \ ^2F_{7/2}$	2.2

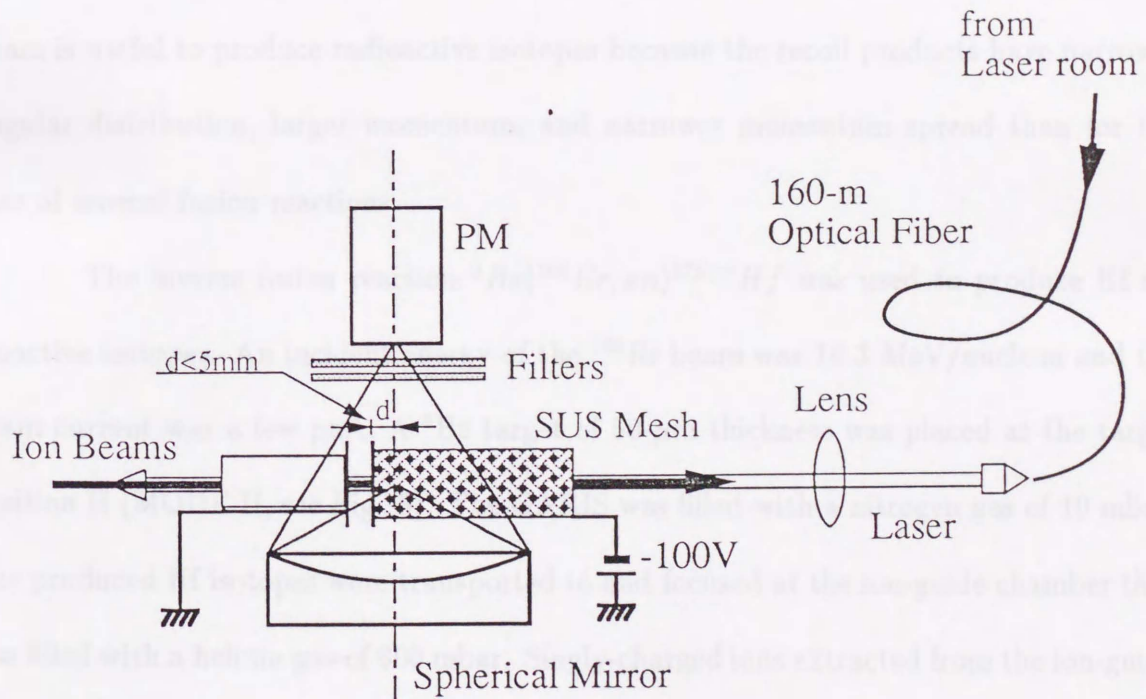


Figure 10: A schematic diagram of the LIF detection system for a collinear geometry.

3.6 Production of radioactive isotope of a refractory element: ^{169}Hf

Hf isotopes, which are of a typical refractory element, were chosen for the first on-line collinear laser spectroscopy because of the existence of the famous high-spin isomer.

In a previous paper [16], it was pointed out that the transmission efficiency of GARIS depends strongly on the angular distribution of the recoil products. Table 2 shows efficiencies of the GARIS for different types of nuclear reactions. The difference of the efficiency is mainly caused by the angular distribution of the recoil products. For recoil products having lower momentum, however, the efficiency of GARIS is further reduced by an energy loss and straggling caused by the multiple scattering with gas in the GARIS. Accordingly, the inverse kinematics of a fusion reaction with heavy incident beam is useful to produce radioactive isotopes because the recoil products have narrower angular distribution, larger momentum, and narrower momentum spread than for the case of normal fusion reactions.

The inverse fusion reaction ${}^9\text{Be}({}^{166}\text{Er}, xn){}^{175-x}\text{Hf}$ was used to produce Hf radioactive isotopes. An incident energy of the ${}^{166}\text{Er}$ beam was 16.3 MeV/nucleon and the beam current was a few pA. A ${}^9\text{Be}$ target of 50- μm thickness was placed at the target position II (MODE II, see Fig. 3). The GARIS was filled with a nitrogen gas of 10 mbar. The produced Hf isotopes were transported to and focused at the ion-guide chamber that was filled with a helium gas of 600 mbar. Singly-charged ions extracted from the ion-guide chamber were accelerated to 30 keV. The accelerated ion beams of the Hf isotopes were stopped with an aluminum foil and accumulated. After about 10-minutes accumulation, γ rays from the decay of Hf isotopes were measured with a Ge(Li) detector. The 492.9-keV

Table 2: Efficiencies of the GARIS for various reactions.

Reaction	Incident Energy	Efficiency
$^{169}\text{Tm}(^{40}\text{Ar}, xn)$	fusion reaction 5 MeV/nucleon	$15 \pm 1 \%$
$^{181}\text{Ta}(^{40}\text{Ar}, \alpha xn)$	fusion reaction 6 MeV/nucleon	$5.3 \pm 0.4 \%$
$^{nat}\text{W}(^{14}\text{N}, X)^{169}\text{Hf}$	target fragmentation 35 MeV/nucleon	$0.5 \pm 0.1 \%$

γ rays from the decay of ^{169}Hf ($T_{1/2} = 3.26$ m) were clearly identified. This is the first measurement of isotopically separated radioactive atomic beams of refractory elements.

4 Results and discussion

4.1 LIF spectrum of Ar^{1+}

Figure 11 shows a typical LIF spectrum measured for 180° incidence at a helium gas pressure (P_{tc}) of 100 mbar, a skimmer voltage (V_{sk}) of -500 V and an acceleration potential (U) of 30 kV. The scanning speed of the laser was 9 s/GHz and the dwell time for photon counting 0.5 s/ch. The FWHM of the spectrum is about 1.4 GHz. We repeated the measurement ten times, and determined the FWHM to be 1.45 ± 0.06 GHz.

4.2 Velocity spread and beam divergence

The skimmer potential dependence of the linewidth of the LIF spectrum was systematically measured for three incident angles (30° , 90° and 180°) at a helium gas pressure of 20 mbar. The results of the investigation are shown in fig. 12. The solid lines are the linear least-squares fit for each incident angle as a function of V_{sk} .

To first order of β , it is enough to measure the linewidth of the LIF spectrum at collinear geometry only to deduce the velocity spread of ion beams. We carefully examined, however, the second order effects of the β , $\delta\beta$ and $\delta\theta$. Since linewidths were measured for three incident angles at a given V_{sk} , the $\delta\beta$ and the $\delta\theta$ are deduced using least-squares fits to eqs. (3) and (9), which are the approximation to second order of $\delta\beta$ and $\delta\theta$. The results of the fittings are plotted in fig. 13. The open circles indicate $\delta\beta/\beta$ and open squares $\delta\theta$.

For the $^{40}\text{Ar}^{1+}$ beam with a kinetic energy of 30 keV, the velocity of the ions is $\beta = 1.3 \times 10^{-3}$ and the orders of magnitudes of $\delta\beta$ and $\delta\theta$ are 10^{-6} and 10^{-3} rad. Accordingly, it is concluded that the approximation to first order is sufficient to calculate the velocity and

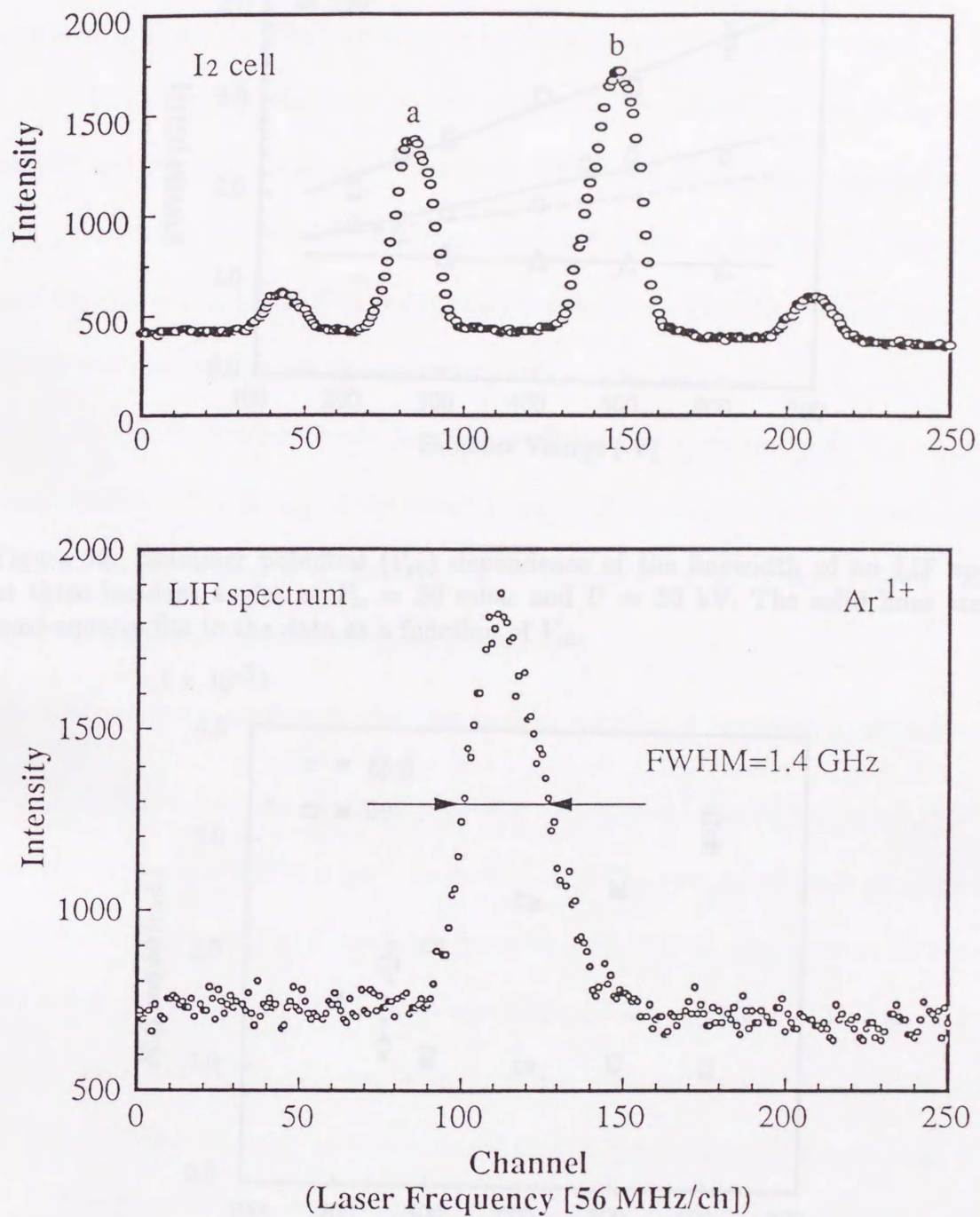


Figure 11: LIF spectrum for the metastable state of Ar¹⁺ ions at 180° incidence. The condition of the IGISOL was as follows: $V_{sk} = -500$ V, $P_{tc} = 100$ mbar and $U = 30$ kV. A reference spectrum of I₂ molecule was measured simultaneously. The wave numbers of the peaks of I₂ spectrum are 16328.1875 cm⁻¹ and 16328.3072 cm⁻¹, respectively [28].

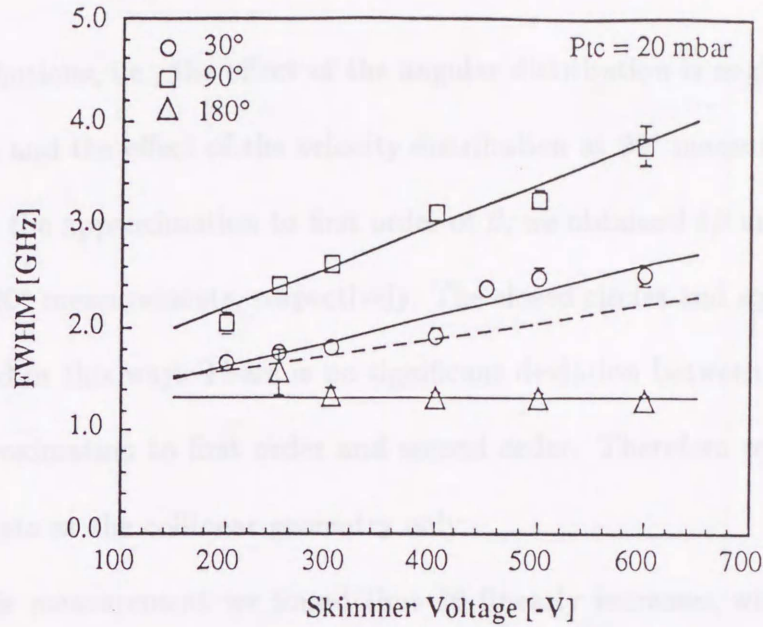


Figure 12: Skimmer potential (V_{sk}) dependence of the linewidth of an LIF spectrum at three incident angles at $P_{tc} = 20$ mbar and $U = 30$ kV. The solid lines are linear least-squares fits to the data as a function of V_{sk} .

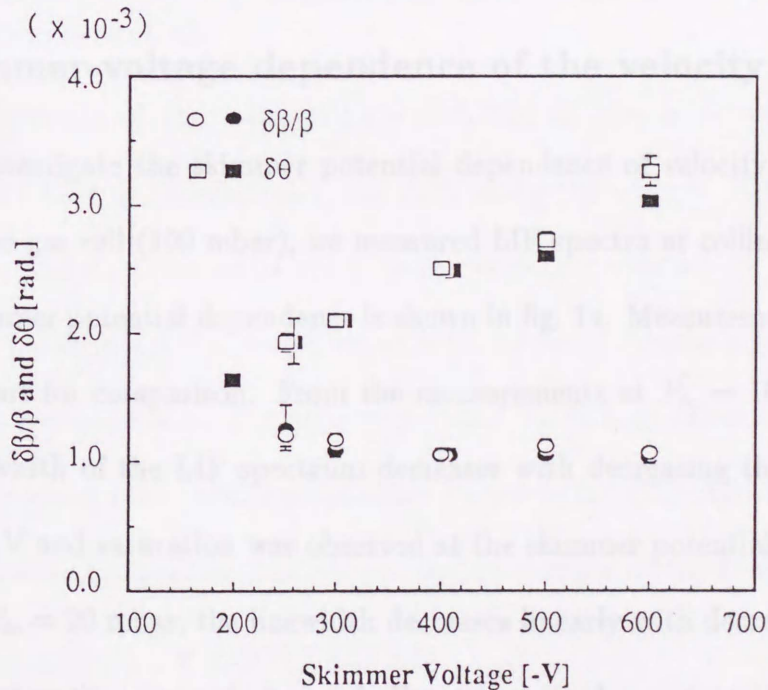


Figure 13: Skimmer potential dependence of $\delta\beta/\beta$ and $\delta\theta$ at $P_{tc} = 20$ mbar. The open circles and squares were deduced from measurements at three incident angles using least-squares fits to second order. The closed circles and squares are derived directly from the measurements at the incidence of 90° and 180° using the approximation to first order.

angular distributions, i.e., the effect of the angular distribution is negligible for collinear measurements and the effect of the velocity distribution at 90° measurements.

Using the approximation to first order of β , we obtained $\delta\beta$ and $\delta\theta$ directly from the 180° and 90° measurements, respectively. The closed circles and squares shown in fig. 13 are deduced in this way. There is no significant deviation between the plots deduced from the approximation to first order and second order. Therefore we can safely derive $\delta\beta$ from the data at the collinear geometry only.

In this measurement we found that $\delta\theta$ linearly increases with V_{sk} while $\delta\beta$ is rather constant. The change of the beam divergence is due to the change of the emittance of the ion beam caused by a lens effect of the skimmer. In other words, more scattered ions are collected at a higher skimmer potential.

4.3 Skimmer-voltage dependence of the velocity spread

To investigate the skimmer potential dependence of velocity spread at a usual pressure in the gas cell (100 mbar), we measured LIF spectra at collinear geometry. The observed skimmer potential dependence is shown in fig. 14. Measurement at 20 mbar was also carried out for comparison. From the measurements at $P_{tc} = 100$ mbar, we found that the linewidth of the LIF spectrum decreases with decreasing the skimmer voltage less than 500 V and saturation was observed at the skimmer potential more than 600 V.

For $P_{tc} = 20$ mbar, the linewidth decreases linearly with decreasing the skimmer voltage and saturation was not observed. Here we noticed a systematic shift in the measurements at $P_{tc} = 20$ mbar between this measurement and that mentioned in section 4.3. The difference between them was only the alignment of the IGISOL: the alignment of the exit hole, the skimmer and the extractor. This shows that the geometrical setup of the

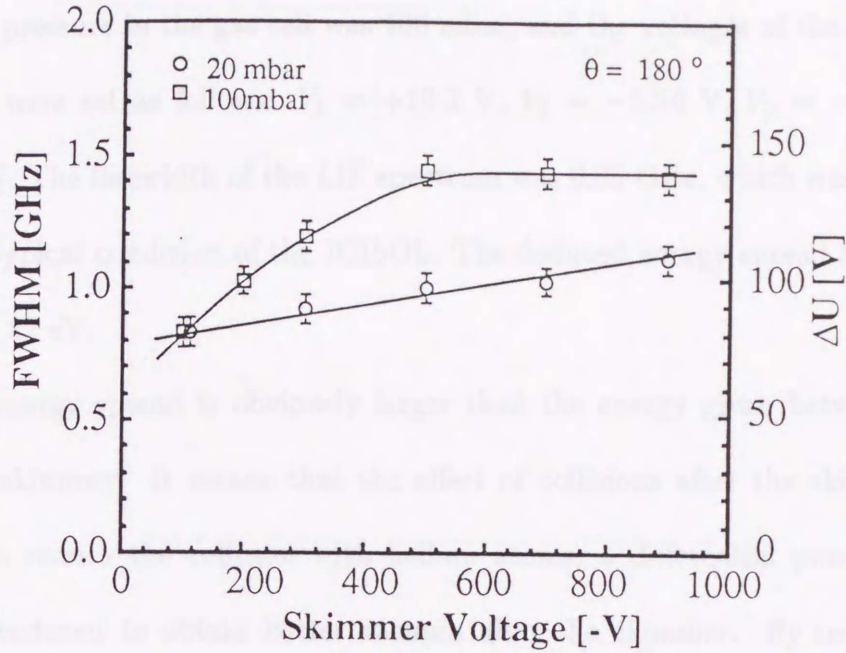


Figure 14: Skimmer potential dependence of the linewidth of an LIF spectrum observed in the collinear geometry. A deduced instability of the acceleration potential (ΔU) is given on the right ordinate.

IGISOL sensitively affects to the velocity distribution. The scales of the presentations of figs. 12 and 14 are so different that the shift seems quite large. But the shift is actually not so large, and does not affect the present systematic analysis.

As shown in fig. 14, an ion beam with narrower velocity spread was obtained for a lower skimmer potential. The efficiency of the IGISOL to extract radioactive isotopes, however, decreases with reducing the skimmer potential [22]. Accordingly, it is not easy to obtain intense radioactive ions with a narrow velocity distribution.

4.4 The effect of SQUEEZER

A new focusing device SQUEEZER enables us to extract ion beams with a low skimmer potential without losing the efficiency of the IGISOL [26]. We have introduced this device into our IGISOL and measured an LIF spectrum of the Ar^{1+} beam from the

IGISOL. The pressure in the gas cell was 100 mbar, and the voltages of the SQUEEZER and skimmer were set as follows: $V_1 = +10.2$ V, $V_2 = -5.54$ V, $V_3 = -2.24$ V, and $V_{s,k} = -10.0$ V. The linewidth of the LIF spectrum was 0.85 GHz, which was about 60 % of that for a typical condition of the IGISOL. The deduced energy spread from the LIF spectrum was 82 eV.

The energy spread is obviously larger than the energy given between the exit hole and the skimmer. It means that the effect of collisions after the skimmer is not negligible. To reduce the collision with helium atoms, a differential pumping system should be introduced to obtain better vacuum after the skimmer. By improving this system, we expect that the energy spread can be reduced to less than 20 eV, which corresponds to a linewidth of about 200 MHz.

4.5 He-gas pressure dependence of the velocity spread

To investigate the He-gas pressure dependence of the velocity spread, measurement was carried out at $V_{s,k} = -500$ V, which is generally used for an ordinary ion guide. The results of the measurement are shown in fig. 15. The linewidth of the LIF spectra decreases sharply below 200 mbar with decreasing the P_{tc} and is nearly constant above 200 mbar.

To obtain a narrower energy spread, operation of the IGISOL with low gas-cell pressure is needed. However, the efficiency of the IGISOL decreases for low gas-cell pressure [16]. Therefore it is difficult to reduce the helium gas pressure in the gas cell so much.

The energy spread of the ion beam from the IGISOL is caused by collisions with helium atoms outside the gas cell. We have, therefore, two ways to reduce the

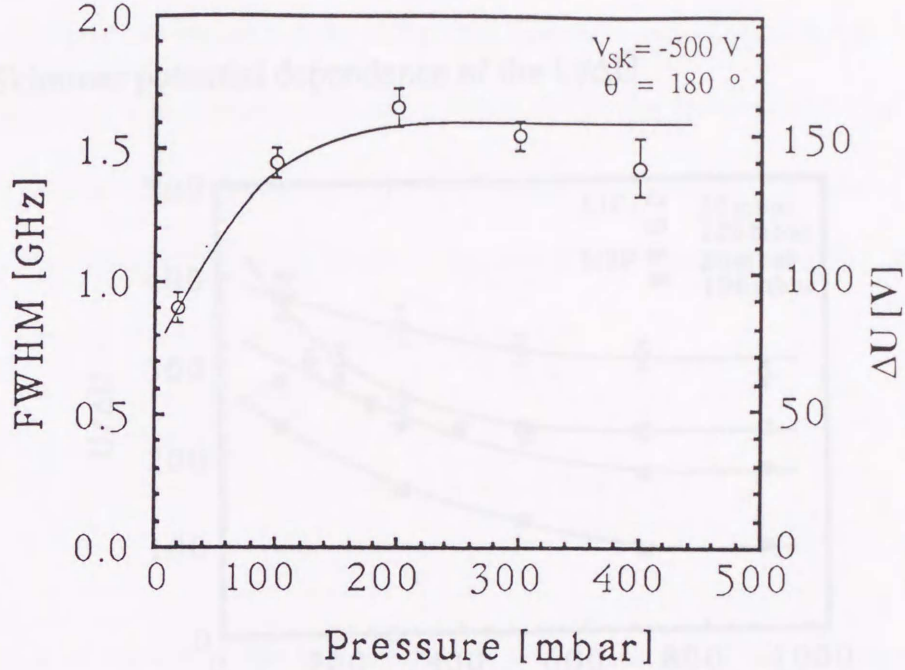


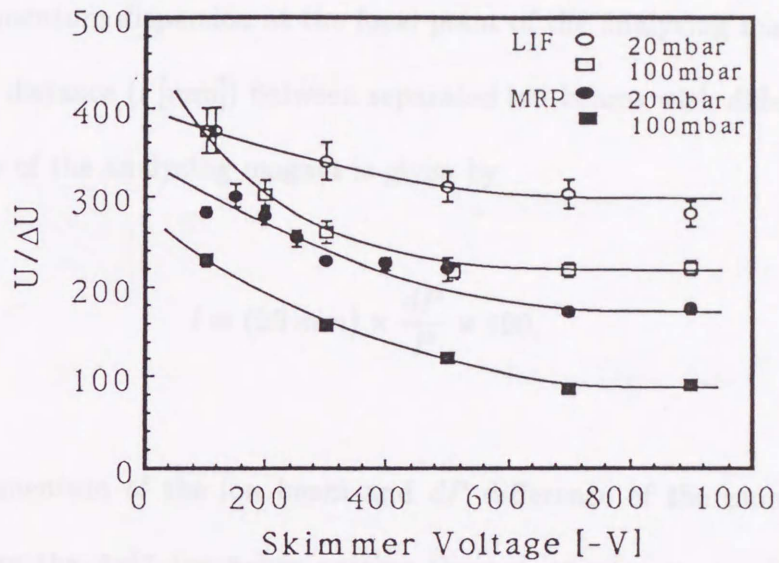
Figure 15: Gas pressure (P_{tc}) dependence of the linewidth of an LIF spectrum observed in the collinear geometry. A deduced instability of the acceleration potential (ΔU) is given on the right ordinate.

energy spread. One is the improvement of the vacuum system. The other is to transport radioactive ions with low potentials, i.e., SQUEEZER.

4.6 Comparison with the mass resolving power

The skimmer-potential and the pressure dependences of the mass resolving power (MRP) were also measured. The mass spectrum was measured at the focal point of the analyzing magnet using a Faraday-cup, which is placed just behind a 1-mm slit as shown in fig. 8. The values of the $U/\Delta U$ are deduced from the results of the measurement of MRP and Doppler broadening using eqs. (13) and (16), and the results are shown in fig. 16. In both cases, the values of the $U/\Delta U$ deduced from the MRP and Doppler broadening have the same tendency, and the absolute value of the $U/\Delta U$ deduced from the Doppler broadening is about two times larger than that from the MRP.

(a) Skimmer potential dependence of the $U/\Delta U$



(b) He-gas pressure dependence of the $U/\Delta U$

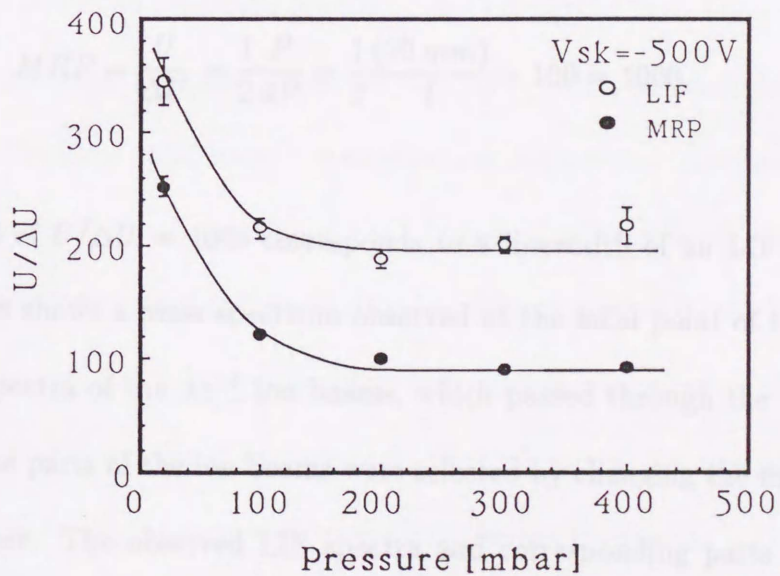


Figure 16: Skimmer-potential and pressure dependences of the $U/\Delta U$ deduced from the mass resolving power and the Doppler broadening: (a) skimmer potential (V_{sk}) dependence; and (b) He-gas pressure (P_{tc}) dependence.

To elucidate the reason for the difference, measurement of the Doppler broadening of the LIF spectrum was carried out using a 1-mm slit at the focal point of the analyzing magnet. The momentum dispersion at the focal point of the analyzing magnet is 20 mm per percent. The distance (l [mm]) between separated ion beams with different momenta at the focal plane of the analyzing magnet is given by

$$l = (20 \text{ mm}) \times \frac{dP}{P} \times 100, \quad (17)$$

where P is a momentum of the ion beam and dP difference of the momentum. (See fig. 17.) Therefore the Ar^{1+} ion beam passing through the 1-mm slit should have an energy spread of 1000 in terms of $U/\Delta U$.

$$MRP = \frac{U}{\Delta U} = \frac{1}{2} \frac{P}{dP} = \frac{1}{2} \frac{(20 \text{ mm})}{l} \times 100 = 1000.$$

The energy spread of $U/\Delta U = 1000$ corresponds to a linewidth of an LIF spectrum of 0.3 GHz. Figure 18 shows a mass spectrum observed at the focal point of the analyzing magnet and LIF spectra of the Ar^{1+} ion beams, which passed through the 1-mm slit at the focal point. The parts of the ion beams were selected by changing the magnetic field of the mass analyzer. The observed LIF spectra and corresponding parts of the mass spectrum are shown in fig. 18: (a) the magnetic field was fixed at the peak of the mass spectrum; and (b,c) the field was fixed at the half maximum. This experiment was carried out under the usual condition of the IGISOL, i.e., $V_{sk} = -500 \text{ V}$ and $P_{tc} = 100 \text{ mbar}$.

In this experiment, we found a discrepancy between experimentally observed

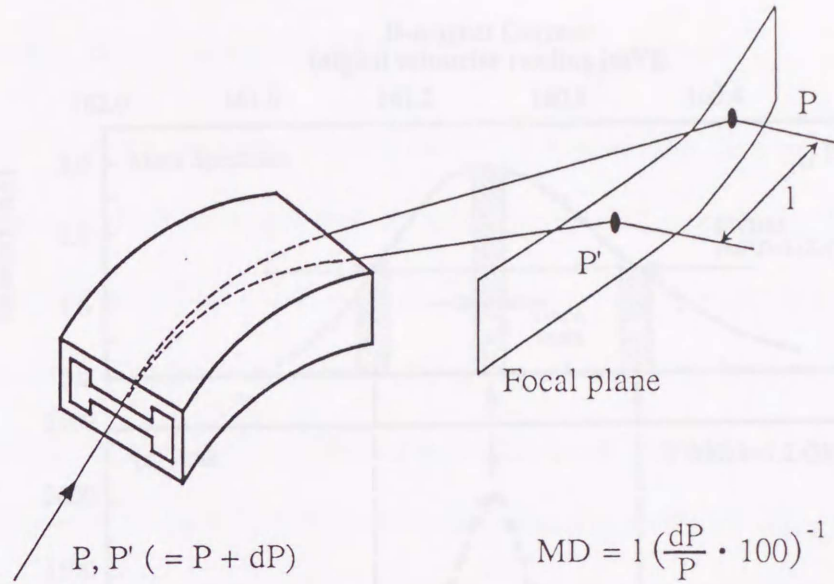


Figure 17: The definition of the momentum dispersion (MD) of an analyzing magnet. The value l is a distance of analyzed ion beams of momenta p and $p' (= P + dP)$ at the focal plane.

linewidth and the linewidth predicted from the mass spectrum: first, the observed Doppler broadening is much larger than the predicted value (0.3 GHz), which is deduced from the size of the slit at the focal point using the momentum dispersion of the analyzing magnet; second, a difference of the peak position of the LIF spectrum associated with the parts (b) and (c) is about two times smaller than that deduced from the MRP (the MRP is 113 and the expected value is 2.7 GHz), and the observed value is very close to the value of the linewidth observed without the slit (about 1.4 GHz). However, the prediction was made using eq. (16) that is obtained by assuming that the MRP depends on the momentum spread only. Accordingly, it is understandable that the value of the $U/\Delta U$ derived from the mass spectrum is smaller than that from the LIF spectrum. Here, we conclude that the value of $U/\Delta U$ deduced from the MRP is considerably underestimated.

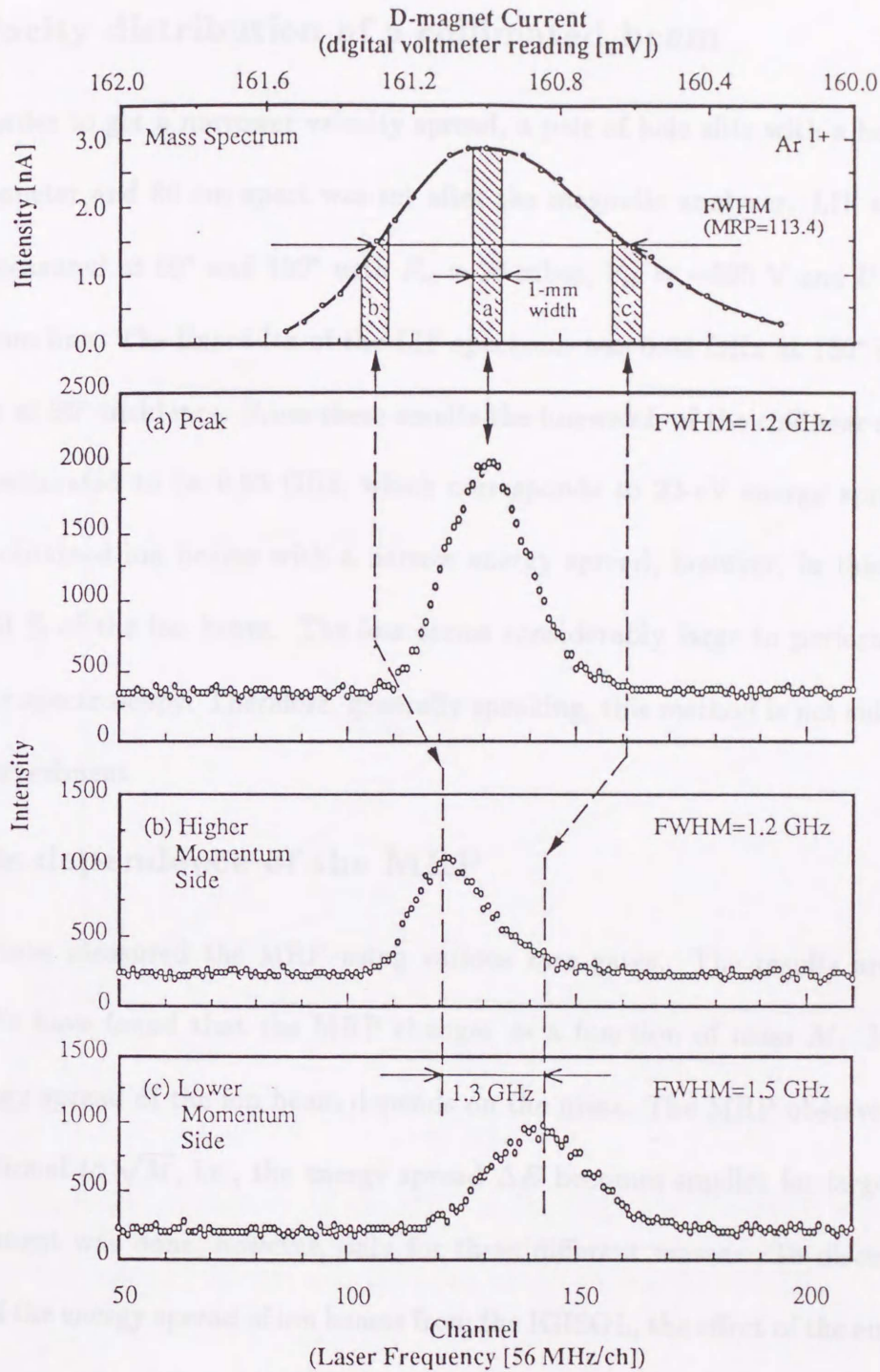


Figure 18: The mass spectrum of Ar^{1+} ions and LIF spectra which correspond to the parts of the ion beams selected with a 1-mm slit at the focal point of the analyzing magnet: (a) LIF spectrum corresponds to the part a (peak) of the mass spectrum; (b) LIF spectrum corresponds to the part b (higher-momentum side) of mass spectrum; and (c) LIF spectrum corresponds to the part c (lower-momentum side) of the mass spectrum.

4.7 Velocity distribution of a collimated beam

In order to get a narrower velocity spread, a pair of hole slits with a hole size of 5 mm in diameter and 80 cm apart was set after the magnetic analyzer. LIF spectra of Ar^{1+} were measured at 90° and 150° with $P_{tc} = 20$ mbar, $V_{sk} = -500$ V and $U = 30$ kV at the 0° beam line. The linewidth of the LIF spectrum was 0.68 GHz at 150° incidence and 1.1 GHz at 90° incidence. From these results the linewidth of the collinear spectrum for Ar^{1+} is estimated to be 0.23 GHz, which corresponds to 22-eV energy spread. We successfully obtained ion beams with a narrow energy spread, however, in this case we lost about 80 % of the ion beam. The loss seems considerably large to perform on-line collinear laser spectroscopy. Therefore, generally speaking, this method is not suitable for the on-line experiment.

4.8 Mass dependence of the MRP

We have measured the MRP using various rare gases. The results are shown in fig. 19. We have found that the MRP changes as a function of mass M . It means that the energy spread of the ion beam depends on the mass. The MRP observed seems to be proportional to \sqrt{M} , i.e., the energy spread ΔE becomes smaller for larger mass. The measurement was done, however, only for three different masses. To discuss mass dependence of the energy spread of ion beams from the IGISOL, the effect of the emittance should also be considered for each mass. Therefore we shall not discuss about the mass dependence of the energy spread here in detail.

Table 2: Estimated yield of radioactive III isotopes from GARIS/IGISOL. The values marked by an asterisk (*) are estimated from experimental data obtained for the $^{88}\text{Sr}(^{208}\text{Pb},\gamma)^{208}\text{Tl}$ reaction [16].

Isotope	Yield (^{208}Pb beam, 10^{12} p.p.a.)
^{208}Tl	1.5
^{209}Bi	1.5
^{210}Po	1.5
^{211}Po	1.5
^{212}Po	1.5
^{213}Po	1.5
^{214}Po	1.5
^{215}Po	1.5
^{216}Po	1.5
^{217}Po	1.5
^{218}Po	1.5
^{219}Po	1.5
^{220}Po	1.5
^{221}Po	1.5
^{222}Po	1.5
^{223}Po	1.5
^{224}Po	1.5
^{225}Po	1.5
^{226}Po	1.5
^{227}Po	1.5
^{228}Po	1.5
^{229}Po	1.5
^{230}Po	1.5
^{231}Po	1.5
^{232}Po	1.5
^{233}Po	1.5
^{234}Po	1.5
^{235}Po	1.5
^{236}Po	1.5
^{237}Po	1.5
^{238}Po	1.5
^{239}Po	1.5
^{240}Po	1.5
^{241}Po	1.5
^{242}Po	1.5
^{243}Po	1.5
^{244}Po	1.5
^{245}Po	1.5
^{246}Po	1.5
^{247}Po	1.5
^{248}Po	1.5
^{249}Po	1.5
^{250}Po	1.5
^{251}Po	1.5
^{252}Po	1.5
^{253}Po	1.5
^{254}Po	1.5
^{255}Po	1.5
^{256}Po	1.5
^{257}Po	1.5
^{258}Po	1.5
^{259}Po	1.5
^{260}Po	1.5
^{261}Po	1.5
^{262}Po	1.5
^{263}Po	1.5
^{264}Po	1.5
^{265}Po	1.5
^{266}Po	1.5
^{267}Po	1.5
^{268}Po	1.5
^{269}Po	1.5
^{270}Po	1.5
^{271}Po	1.5
^{272}Po	1.5
^{273}Po	1.5
^{274}Po	1.5
^{275}Po	1.5
^{276}Po	1.5
^{277}Po	1.5
^{278}Po	1.5
^{279}Po	1.5
^{280}Po	1.5
^{281}Po	1.5
^{282}Po	1.5
^{283}Po	1.5
^{284}Po	1.5
^{285}Po	1.5
^{286}Po	1.5
^{287}Po	1.5
^{288}Po	1.5
^{289}Po	1.5
^{290}Po	1.5
^{291}Po	1.5
^{292}Po	1.5
^{293}Po	1.5
^{294}Po	1.5
^{295}Po	1.5
^{296}Po	1.5
^{297}Po	1.5
^{298}Po	1.5
^{299}Po	1.5
^{300}Po	1.5

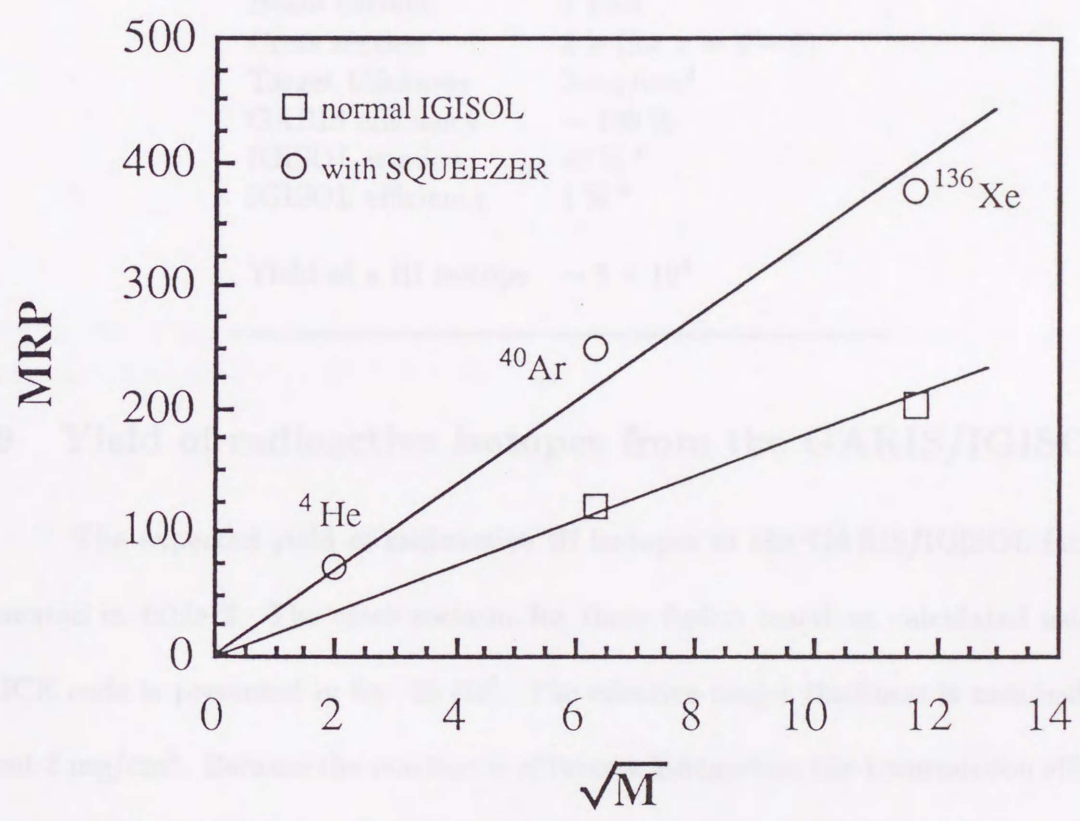


Figure 19: The mass dependence of the MRP of the IGISOL. The MRP was measured for ^4He , ^{40}Ar and ^{136}Xe . The abscissa is a square root of mass M . The open squares were measured with a normal IGISOL, and the open circles with a SQUEEZER.

Table 3: Expected yield of radioactive Hf isotopes from GARIS/IGISOL. The values marked by an asterisk (*) are estimated from experimental data obtained for the $^{141}\text{Pr}(^{40}\text{Ar}, 5n)^{176}\text{Ir}$ reaction [16].

Reaction	${}^9\text{Be}({}^{166}\text{Er}, xn)^{175-x}\text{Hf}$
Beam current	1 pA
Cross section	1 b (for $x = 4 - 9$)
Target thickness	3 mg/cm^2
GARIS efficiency	$\sim 100 \%$
IGISOL window	40 % *
IGISOL efficiency	1 % *
Yield of a Hf isotope	$\sim 5 \times 10^3$

4.9 Yield of radioactive isotopes from the GARIS/IGISOL

The expected yield of radioactive Hf isotopes at the GARIS/IGISOL facility is presented in table 3. The cross sections for these fusion reactions calculated using the ALICE code is presented in fig. 20 [29]. The effective target thickness is assumed to be about 3 mg/cm^2 . Because the reaction is of inverse kinematics, the transmission efficiency of the GARIS is expected to be almost 100 %. At the entrance window of the gas cell of the IGISOL, about 40 % of the products pass through the window because the beam size at the focal point of the GARIS is larger than the size of the window [16]. The extraction efficiency of the IGISOL is about 1 % [16]. The yield of a Hf isotope is thus estimated to be 5×10^3 particles/s for the fusion reaction ${}^9\text{Be}({}^{166}\text{Er}, xn)^{175-x}\text{Hf}$, $x = 4 - 9$, at an ${}^{166}\text{Er}$ beam current of 1 pA. (Actual beam intensity is expected to be 5 pA or even more.)

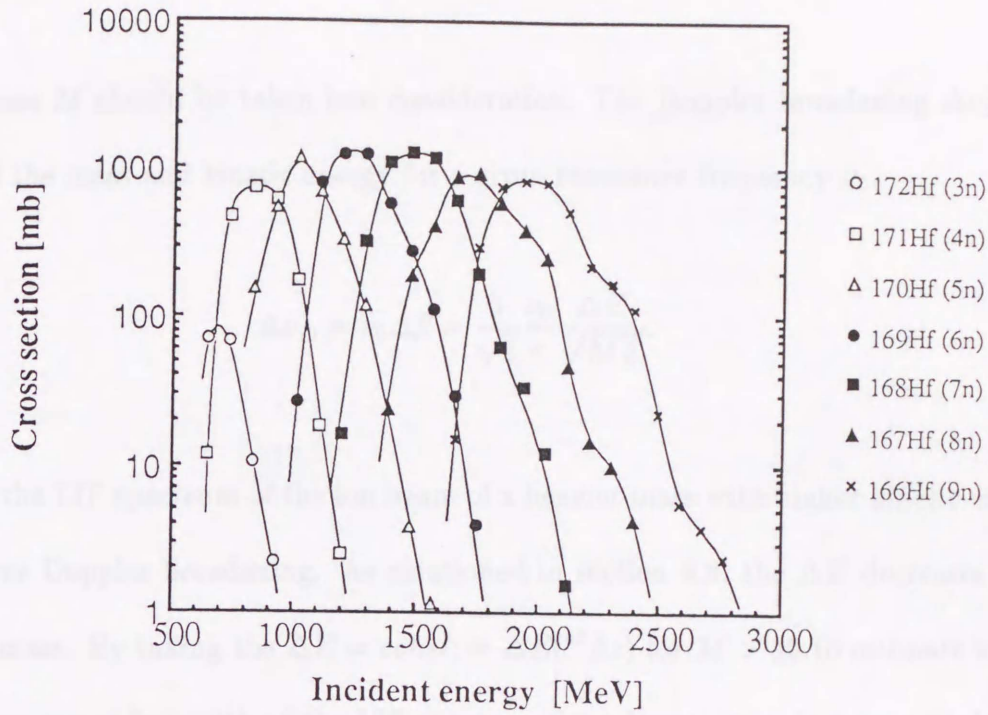


Figure 20: The cross sections of the fusion reactions for ${}^9\text{Be}({}^{166}\text{Er}, xn){}^{175-x}\text{Hf}$, which are calculated using the ALICE code [29].

The observed yield of ${}^{169}\text{Hf}$ (extracted from the GARIS/IGISOL and accelerated to 30 keV) was about 100 particles/s for an ${}^{166}\text{Er}$ beam current of 1 pA. The helium gas pressure used in the gas cell was $P_{tc} = 600$ mbar.

The observed yield was considerably smaller than the estimated one. There are several reasons accounting for this reduction: (1) the He-gas pressure in the gas cell was too low to stop all of the produced ${}^{169}\text{Hf}$ ions; and (2) the IGISOL system was not yet completely optimized. These problems will be solved in due course.

4.10 Feasibility of on-line collinear laser spectroscopy

We have systematically measured the velocity spread of the ion beam from the IGISOL. The linewidth of the spectrum for Ar^{1+} at the collinear geometry was about 1.4 GHz for the typical IGISOL condition: $P_{tc} = 100$ mbar, $V_{sk} = -500$ V, and $U = 30$ kV. It seems still inadequate to do collinear spectroscopy. For heavier element, however, the

effect of mass M should be taken into consideration. The Doppler broadening $\Delta\nu_D$ is a function of the mass and kinetic energy for a given resonance frequency ν_0 .

$$\Delta\nu_D = \nu_0 \Delta\beta = \frac{1}{\sqrt{2}} \frac{\nu_0}{c} \frac{\Delta E}{\sqrt{ME}}. \quad (18)$$

Therefore, the LIF spectrum of the ion beam of a heavier mass with higher kinetic energy has narrower Doppler broadening. As mentioned in section 4.8, the ΔE decreases with increasing mass. By taking the $\Delta E = \text{const.} = \Delta E(^{40}\text{Ar})$ for $M > 40$ to estimate safely, we have a narrower linewidth of the LIF spectrum for a heavy-mass isotope with higher kinetic energy. For example, a linewidth of about 500 MHz is expected for $M = 160$ and $E = 50$ keV. Thus we conclude that in the region from Lu to Ir, collinear laser spectroscopy with the RIKEN GARIS/IGISOL is quite feasible without a SQUEEZER.

As shown in section 4.4, the new focusing device SQUEEZER was successfully introduced. The energy spread observed was about 80 eV, and we can reduce it to less than 20 eV by introducing a differential pumping system. Therefore, for heavy isotopes with $M > 100$, we expect the resonance linewidth of about 100 MHz at $U = 50$ kV. This linewidth is narrow enough to carry out on-line collinear laser spectroscopy.

The estimated yield of a Hf isotope is 5×10^3 particles/s for a fusion reaction of ${}^9\text{Be}({}^{166}\text{Er}, xn){}^{175-x}\text{Hf}$ at an ${}^{166}\text{Er}$ beam current of 1 pA, as shown in section 4.9. Since the actual ${}^{166}\text{Er}$ incident beam intensity from the RIKEN ring cyclotron facility is a few pA, we can expect a few times more intense radioactive isotope beam. Generally speaking, however, such a low yield requires detection techniques of higher sensitivity. A number of rich techniques have been developed [7].

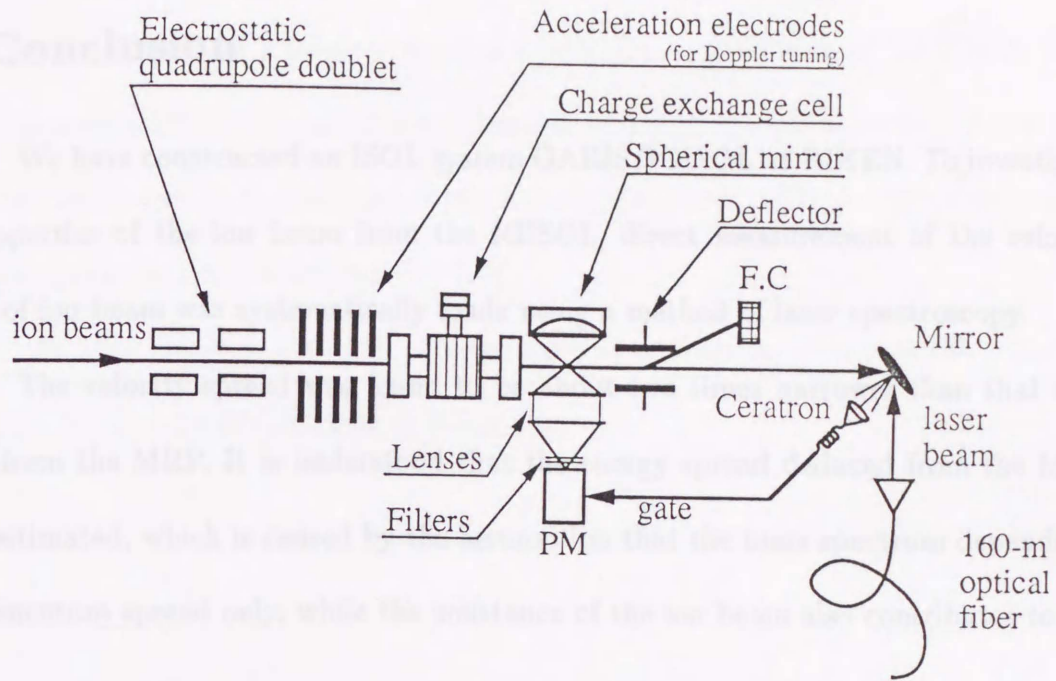


Figure 21: The arrangement for coincidence collinear laser spectroscopy. The arrival of atoms is detected with a Ceratron that detects the secondary electrons emitted when the particle strikes on an aluminum-coated mirror.

The sensitivity of the collinear laser spectroscopy is limited mainly by background from stray laser light, radioactivity, noise of photomultiplier, and so on [7]. To suppress the background, a photon-particle coincidence method was developed by a group of Daresbury Laboratory [30]. The sensitivity of the collinear laser spectroscopy with this system was increased by several order of magnitude [30]. In fact, they successfully made collinear laser spectroscopy with a ^{87}Sr beam of about 100 particles/s [31]. Figure 21 shows our experimental arrangement for the photon-particle coincidence method. This system is ready to be tested at RIKEN.

5 Conclusion

We have constructed an ISOL system GARIS/IGISOL at RIKEN. To investigate the properties of the ion beam from the IGISOL, direct measurement of the velocity spread of ion beam was systematically made using a method of laser spectroscopy.

The velocity spread was found to be about two times narrower than that estimated from the MRP. It is understood that the energy spread deduced from the MRP is overestimated, which is caused by the assumption that the mass spectrum depends on the momentum spread only, while the emittance of the ion beam also contributes to the MRP.

The linewidth of the LIF spectrum observed for Ar^{1+} was about 1.4 GHz at present for a usual IGISOL condition: $V_{sk} = -500$ V, $P_{tc} = 100$ mbar, and $U = 30$ kV. The energy spread corresponding to the linewidth is 135 eV. We have shown that for heavy isotopes with a high kinetic energy, the linewidth will become narrower and on-line collinear laser spectroscopy is possible. It is also shown that the SQUEEZER works to reduce the velocity spread of the ion beam significantly. The effectiveness of introducing a differential pumping system is pointed out.

From the experimental data and theoretical consideration, the experimental linewidth of an LIF spectrum is about 100 MHz for a radioactive isotope with a mass $M > 100$ at $U = 50$ kV. This linewidth is narrow enough to perform high-resolution laser spectroscopy of atomic nuclei.

The inverse kinematics of fusion reactions, ${}^9\text{Be}({}^{166}\text{Er}, xn){}^{175-x}\text{Hf}$, was exploited to produce radioactive Hf isotopes. The radioactive isotope ${}^{169}\text{Hf}$ was successfully extracted from the GARIS/IGISOL and accelerated up to 30 keV. The yield of ${}^{169}\text{Hf}$ was

about 100 particles/s for a beam current of 1 pA. By optimization of GARIS/IGISOL, it is expected that the yield will be several ten times larger than that presently observed. This yield of the radioactive isotopes is much enough to make collinear laser spectroscopy when we apply the coincidence method [30].

We thus conclude that the collinear laser spectroscopy of radioactive refractory elements with the GARIS/IGISOL is promising.

The $5f_{5/2}$ - $5f_{7/2}$ transition from the $5f_{7/2}^2 \ ^3F_4$ ground state to the $5f_{5/2}^2 \ ^3D_3$ state in Hf atoms was observed. According to A. Weysser and G. Ziegler [31], the excited Hf atoms decay preferentially to the $5f_{5/2}^2 \ ^3F_4$ state, thereby emitting a photon of 234.09-nm wavelength. The energy levels associated with the measurement is shown in fig. 25. A band-pass filter (Kodak BP-72) and two sharp-cut filters (Kodak R-04 and R-05) were set in front of the excited photomultiplier (Hamamatsu R333-02) in order to suppress the fluorescence light selectively and to reduce the background. The signal from the photomultiplier was recorded as a function of time using a microcomputer (NEC-

Appendix A

Collinear laser spectroscopy setup for on-line experiment

We have constructed a setup for collinear fast atomic-beam laser spectroscopy and placed it at the 0° beam line of the IGISOL. To establish this system, we made a collinear laser spectroscopy with stable Hf isotope. A schematic diagram of this system is shown in fig. 22. Instead of the ion-guide gas cell, a Hf metallic plate was placed at the position of the exit hole of the gas cell, and Hf ions were produced by the irradiation of the high power frequency-doubled output of a pulsed Nd:YAG laser (LUMONICS mini-Q Nd:YAG laser). The Nd:YAG laser used was at a wavelength of 523 nm and with an output power of about 5 mJ at a repetition rate of 10 Hz. The ions produced were extracted through a collimator, accelerated up to 30 keV and separated with an analyzing magnet. The mass-separated ion beam was transported to the collinear laser spectroscopy system, which consists of a set of acceleration electrodes for Doppler tuning, a charge exchange cell for neutralization of the ion beam and an LIF detection system. The neutralized atomic beam and the laser beam were superimposed collinearly.

The 618.51-nm transition from the $5d^26s^2\ ^3F_2$ ground state to the $5d^26s6p\ ^3D_2$ state in Hf atoms was observed. According to A. Werner and D. Zimmermann [32], the excited Hf atom decays predominantly to the $5d^26s^2\ ^3F_3$ state, thereby emitting a photon of 724.09-nm wavelength. The energy levels associated with the measurement is shown in fig. 23. A band-pass filter (Kenko BP-72) and two sharp-cut filters (Kenko R-64 and R-66) were set in front of the cooled photomultiplier (Hamamatsu R943-02) in order to measure the fluorescence light selectively and to reduce the background. The signal from the photomultiplier was recorded as a function of time using a microcomputer (NEC-

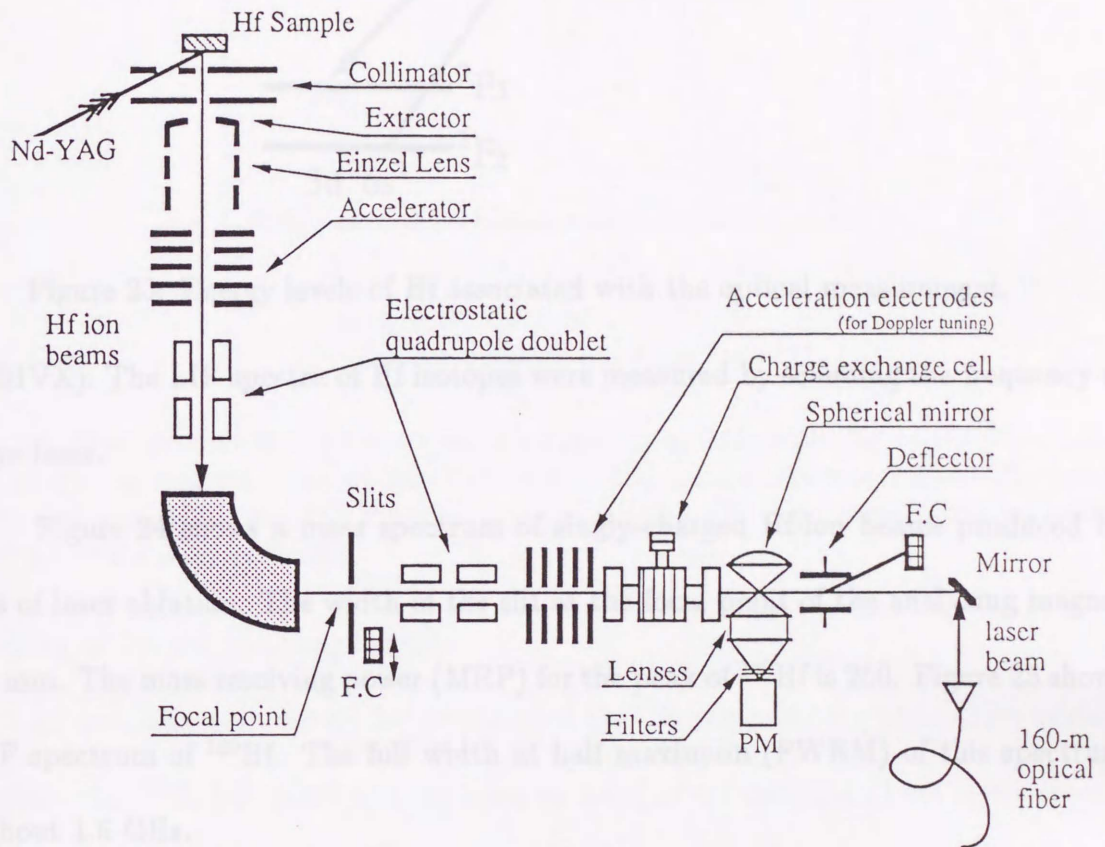


Figure 22: A schematic diagram for collinear laser spectroscopy.

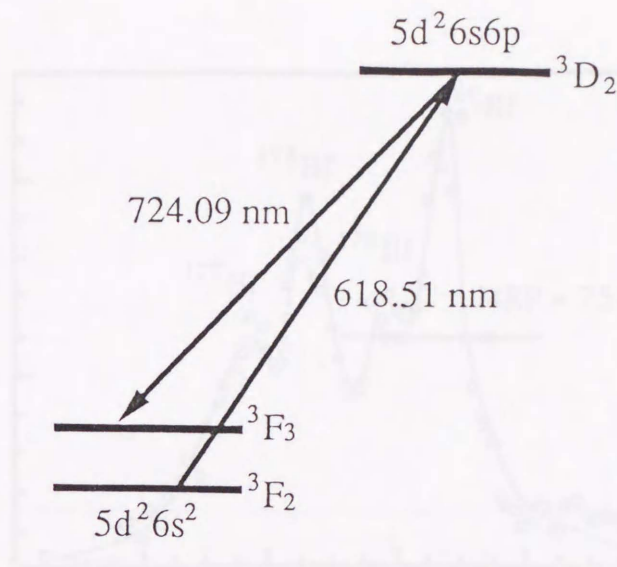


Figure 23: Energy levels of Hf associated with the optical measurement.

PC9801VX). The LIF spectra of Hf isotopes were measured by scanning the frequency of the dye laser.

Figure 24 shows a mass spectrum of singly-charged Hf-ion beams produced by means of laser ablation. The width of the slit at the focal point of the analyzing magnet was 1 mm. The mass resolving power (MRP) for the peak of ^{180}Hf is 250. Figure 25 shows an LIF spectrum of ^{180}Hf . The full width at half maximum (FWHM) of this spectrum was about 1.5 GHz.

The experimental value of ΔU deduced from the MRP of ^{180}Hf is about 120 eV. The value of ΔU deduced from the LIF is about two times larger than that from the MRP. This result is just opposite compared to previous observations (see section 4.6): In general, the ΔU deduced from the MRP should be larger than that from the LIF spectrum, since the MRP depends not only on the momentum distribution of ion beams but also on the emittance. Probably the reason is to be found in the effective sodium vapor pressure (or the product of pressure \times length) in the charge exchange cell. The effective vapor pressure should be optimized to avoid unwanted collisions which cause

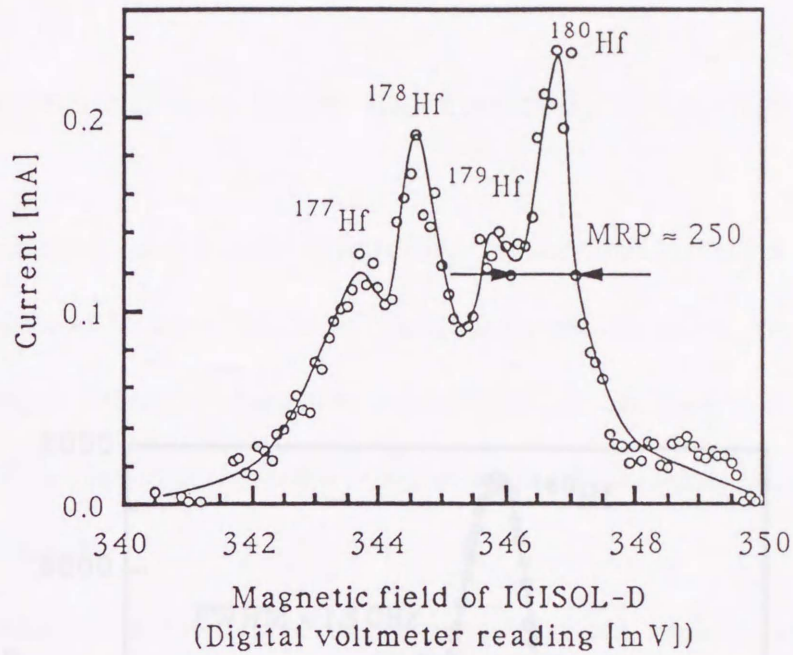


Figure 24: Mass spectrum of Hf isotopes. This spectrum was measured at the focal point of the analyzing magnet. The width of the slit at the focal point was 1 mm. The beam current was measured with the Faraday cup behind the slit. The mass resolving power (MRP) for ^{180}Hf was about 250.

broadening of the resonance linewidth.

In conclusion, it should be emphasized that the apparatus successfully worked to measure the ^{180}Hf LIF spectrum, assuring on-line fast atomic-beam laser spectroscopy with the RIKEN GARIS/IGISOL.

Appendix B

High-resolution off-line laser spectroscopy setup for refractory elements

Before making on-line laser spectroscopy, the atomic structure should be well studied. An apparatus for an off-line laser spectroscopy will, therefore, play an important

role in supporting the study of shielded unstable nuclei. We have thus constructed an apparatus for off-line laser spectroscopy, which is used to study long-lived unstable

nuclei as well as stable nuclei. For an atomic laser spectroscopy, which is used, while the ions are transported

in order to study refractory elements, the atomic structure of the atomic beams of refractory elements is

refractory elements is studied using a laser beam with a shielded high-intensity ion gun

ion gun which is a shielded high-intensity ion gun. The photoelectron is called "spattering".

The photoelectron is called "spattering". The spattering is controlled by the ion gun and the ion gun is controlled by the beam intensity, the spot size of the beam on target, the kinetic energy, species of the spattering ion, and so on. At present, we use Ar-ion beam for spattering. The maximum current of the Ar¹⁴⁺ ion beam from the ion gun is a few nA, and the maximum kinetic energy is 20 keV. The electron beam generated by spattering and the laser beam were perpendicularly in front of

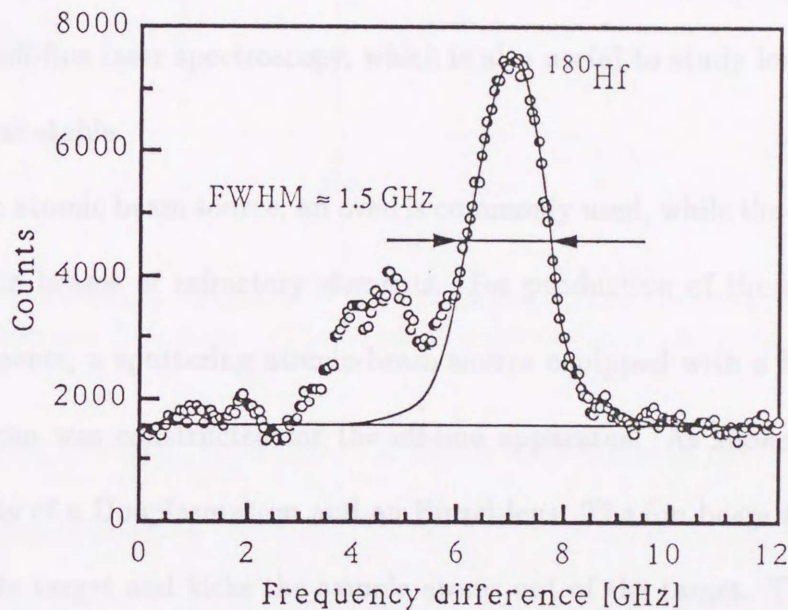


Figure 25: Laser-induced fluorescence (LIF) spectrum of isotope-separated Hf atoms. The magnetic field of the separator was set to maximum transmission of ¹⁸⁰Hf. The width of the slit at the focal point of the analyzing magnet was 1 mm. The FWHM of the main peak of ¹⁸⁰Hf is about 1.5 GHz. The small peaks observed at the lower frequency side of the main peak of ¹⁸⁰Hf are due to contaminations by other Hf isotopes in the ion beam after mass separation.

Appendix B

High-resolution off-line laser spectroscopy setup for refractory elements

Before making on-line laser spectroscopy, the atomic structure should be well studied. An apparatus for an off-line laser spectroscopy will, therefore, play an important role in supporting the study of short-lived unstable nuclei. We have thus constructed an apparatus for off-line laser spectroscopy, which is also useful to study long-lived unstable nuclei as well as stable.

For an atomic beam source, an oven is commonly used, while the oven is impotent to make atomic beams of refractory elements. For production of the atomic beams of refractory elements, a sputtering atomic-beam source equipped with a hand-made high-intensity ion gun was constructed for the off-line apparatus. As shown in fig. 26, the ion gun consists of a Duoplasmatron and an Einzel lens. The ion beam from the ion gun strikes a sample target and kicks the sample atoms out of the target. This phenomenon is called 'sputtering'. The sputtering atomic-beam source is powerful to produce the atomic beams of refractory elements as well as others, because the sputtering process is independent of chemical and physical properties, and the most of the sputtered particles are neutral (more than 90 %) [33]. The conditions of the sputtering ion beam from the ion gun are easily controlled: the beam intensity, the spot size of the beam on target, incident energy, species of the sputtering ion, and so on.

At present, we use Ar-ion beam for sputtering. The maximum current of the Ar¹⁺ ion beam from the ion gun is a few mA, and the maximum kinetic energy is 20 keV. The atomic beam generated by sputtering and the laser beam cross perpendicularly in front of

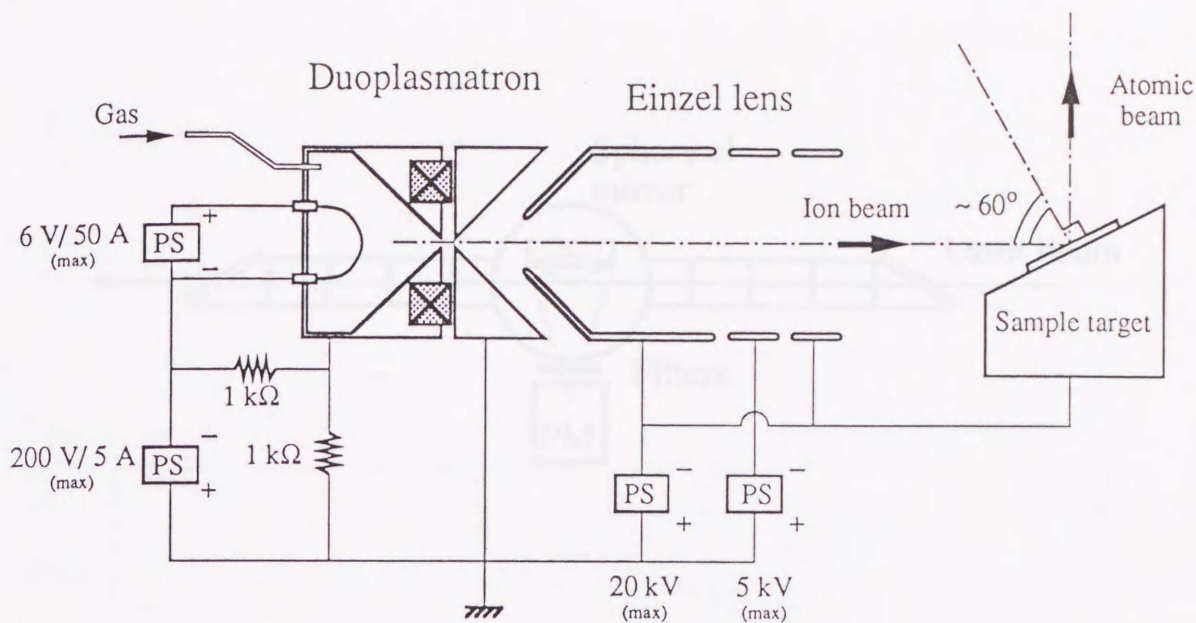


Figure 26: A schematic diagram of the sputtering atomic beam source equipped with Duoplasmatron and Einzel lens. The incident angle of the ion beam to the target is about 60° .

the spherical mirror which is 80 mm in diameter and 60 mm in radius of curvature. The fluorescence lights from the atoms are collected with the spherical mirror. The solid angle of photon collection is 1.14π sr. To reduce the background photons from the laser beam and the sputtering atomic-beam source, baffles are used. Figure 27 shows a schematic diagram of the off-line laser spectroscopy setup.

We successfully observed an LIF spectrum of refractory element ^{nat}Hf with this apparatus. Figure 28 shows the Hf LIF spectrum. The observed transition is the same as the measurement mentioned in appendix A. (The 618.51-nm transition was observed.) The set of the filters and the photomultiplier used were also the same. The observed linewidth of the Hf LIF spectrum is about 20 MHz. This linewidth is good enough to study hyperfine structures.

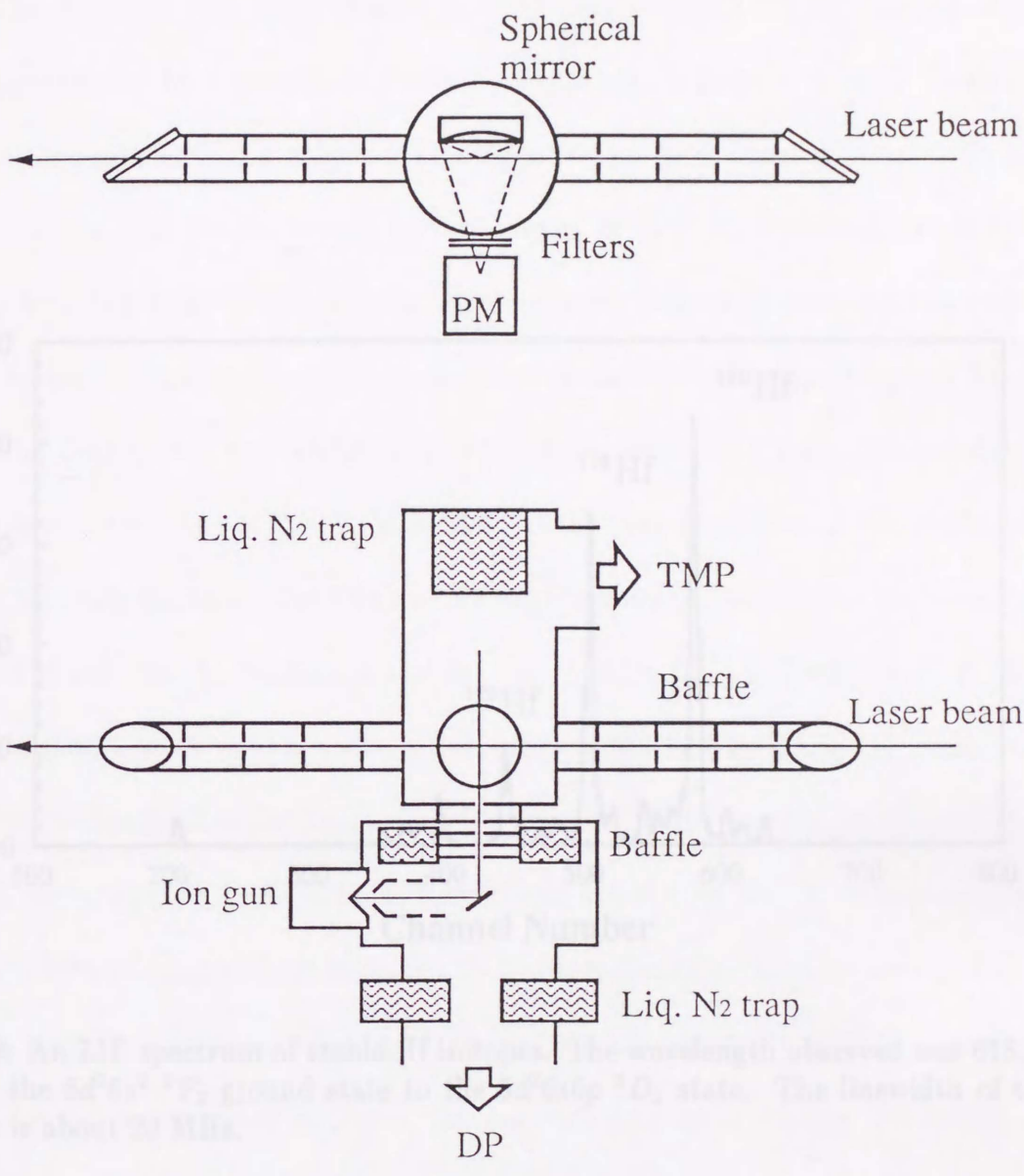


Figure 27: A schematic diagram of the off-line laser spectroscopy setup.

Acknowledgment

The author is very much obliged to many people during the preparation of this thesis. In particular, he is grateful to Prof. Y. Yoshizawa, I. Endo and Dr. T. Aoyama for their encouragements and enlightening discussions at Waseda University. He also wishes to acknowledge the continuous encouragement of Prof. H. Masuhara at RIKEN. He wishes to thank Prof. T.T. Janssen, who began the project of laser spectroscopy at

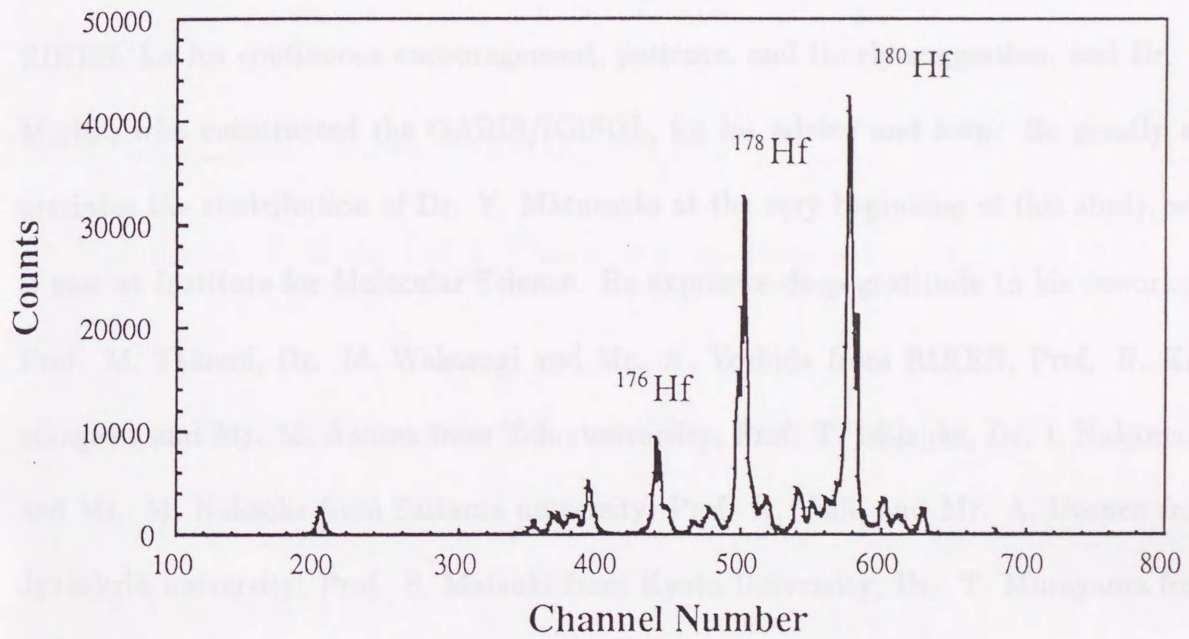


Figure 28: An LIF spectrum of stable Hf isotopes. The wavelength observed was 618.51 nm from the $5d^26s^2\ ^3F_2$ ground state to the $5d^26s6p\ ^3D_2$ state. The linewidth of the spectrum is about 20 MHz.

Acknowledgment

The author is very much obliged to many people during the preparation of this thesis. In particular, he is grateful to Profs. Y. Yoshizawa, I. Endo and Dr. T. Horiguchi for their encouragements and enlightening discussions at Hiroshima university. He also wishes to acknowledge the continuous encouragement of Prof. H. Kamitsubo at RIKEN. He wishes to thank Prof. T.T. Inamura, who began the project of laser spectroscopy at RIKEN, for his continuous encouragement, patience, and timely suggestion, and Dr. K. Morita, who constructed the GARIS/IGISOL, for his advice and help. He greatly appreciates the contribution of Dr. Y. Matumoto at the very beginning of this study, who is now at Institute for Molecular Science. He expresses deep gratitude to his coworkers: Prof. M. Takami, Dr. M. Wakasugi and Mr. A. Yoshida from RIKEN; Prof. H. Katsuragawa and Mr. M. Azuma from Toho university; Prof. T. Ishizuka, Dr. I. Nakamura, and Mr. M. Nakaoka from Saitama university; Prof. K. Valli, and Mr. A. Iivonen from Jyväskylä university; Prof. S. Matsuki from Kyoto University; Dr. T. Murayama from Tokyo university of mercantile marine; Dr. K. Shimomura from Osaka university; Dr. T. Shinozuka from Tohoku university; Dr. I. Sugai from the university of Tokyo; Prof. Y. Tagishi from the university of Tsukuba. He also wishes to thank Messrs. M. Suzuki, H. Kosuga, and M. Takayanagi from Toho university for the assistance in the experiments. He greatly acknowledges the hospitality extended to him during his stay at RIKEN.

References

- [1] N.F. Ramsey, *Molecular Beams* (Oxford University Press, New York, 1956).
- [2] H. Kopfermann, *Nuclear Moments*, Pure and Applied Physics Vol. 2 (Academic Press, New York, 1958).
- [3] W.H. King, *Isotope Shifts in Atomic Spectra* (Plenum Press, New York and London, 1984).
- [4] K. Heilig, *Spectrochimica Acta* 42B (1987) 1237.
- [5] P. Aufmuth, K. Heilig and A. Steudel, *Atomic Data and Nuclear Data Tables* 37 (1987) 455.
- [6] P. Jacquinet and R. Klapisch, *Rep. Prog. Phys.* 42 (1979) 50.
- [7] E.W. Otten, *Treatise on Heavy-Ion Science*, ed. D.A. Bromley, vol. 8 (Plenum Press, New York, 1989) p. 517.
- [8] G. Ulm, S.K. Bhattacharjee, P. Dabkiewicz, G. Huber, H.-J. Kluge, T. Kühl, H. Lochmann, E.-W. Otten, K. Wendt, S.A. Ahmad, W. Klempt, R. Neugart, and the ISOLDE Collaboration, *Z. Phys.* A325 (1986) 247.
- [9] W.C. Ma, A.V. Ramayya, J.H. Hamilton, S.J. Robinson, M.E. Barclay, K. Zhao, J.D. Cole, E.F. Zganjar and E.H. Spejewski, *Phys. Lett.* 139B (1984) 276.
- [10] J.H. Hamilton, *Treatise on Heavy-Ion Science*, ed. D.A. Bromley, Vol.8 (Plenum Press, New York, 1989) p.3.

- [11] J.A. Bounds, C.R. Bingham, P. Juncar, H.K. Carter, G.A. Leander, R.L. Mlekodaj, E.H. Spejewski and W.M. Fairbank, Jr., Phys. Rev. Lett. 55 (1985) 2269.
- [12] U. Krönert, St. Becker, G. Bollen, M. Gerber, Th. Hilberath, H.-J. Kluge, G. Passler, and the ISOLDE Collaboration, Z. Phys. A331 (1988) 521.
- [13] Th. Hilberath, St. Becker, G. Bollen, M. Gerber, H.-J. Kluge, U. Krönert, G. Passler, and the ISOLDE collaborator, Z. Phys. A332 (1989) 107.
- [14] H.L. Ravn and B.W. Allardyce, Treatise on Heavy-Ion Science, ed. D.A. Bromley, Vol.8 (Plenum Press, New York, 1989) p.363.
- [15] K. Morita, T. Inamura, T. Nomura, J. Tanaka, Y. Nagai, A. Yoshida, T. Shinozuka and M. Fujioka, The proceedings of the first international conference on radioactive nuclear beams, ed. W.D. Myers, J.M. Nitschke and E.B. Norman (World Scientific, Singapore, 1990) p. 585.
- [16] K. Morita, A. Yoshida, T.T. Inamura, M. Koizumi, T. Nomura, J. Tanaka, Y. Nagai, T. Toriyama, K. Yoshimura, A. Asai, K. Omata, M. Fujioka, T. Shinozuka, H. Miyatake, K. Sueki, H. Kudo and Y. Hatsukawa, The proceedings of the 1st specialist research meeting on the electromagnetic isotope separators and their applications, ed. M. Fujioka, Y. Kawase and K. Okano (Research Reactor Institute, Kyoto University, 1991) p. 32.
- [17] J. Ärje, Physica Scripta, T3 (1983) 37.
- [18] J. Ärje, J. Äystö, H. Hyvönen, P. Taskinen, V. Koponen, J. Honkanen, A. Hautojärvi and K. Vierinen, Phys. Rev. Lett. 54 (1985) 99.

- [19] M. Koizumi, T.T. Inamura, K. Morita, A. Yoshida, M. Takami, M. Wakasugi, T. Ishizuka, T. Horiguchi, T. Shinozuka, Y. Tagishi, I. Nakamura, M. Nakaoka, T. Murayama, I. Sugai, M. Azuma, H. Katsuragawa, K. Shimomura, S. Matsuki, A. Iivonen and K. Valli, presented at the Int. Symp. on Lasers in Nucl. Phys. (Wako, 1991), and to be published in *Hyp. Int.*
- [20] J. Ärje, J. Äystö, H. Hyvönen, P. Taskinen, V. Koponen, J. Honkanen, K. Valli, A. Hautojärvi and K. Vierinen, *Nucl. Instr. and Meth. A*247 (1986) 431.
- [21] M. Yoshii, H. Hama, K. Taguchi, T. Ishimatsu, T. Shinozuka, M. Fujioka and J. Ärje, *Nucl. Instr. and Meth. B*26 (1987) 410.
- [22] P. Taskinen H. Penttilä, J. Äystö, P. Dendooven, P. Jauho, A. Jokinen and M. Yoshii, *Nucl. Instr. and Meth. A*281 (1989) 539.
- [23] N. Schmidt, Private communication (Diplomarbeit 1989, Mainz university).
- [24] K. Morita, T. Inamura, T. Nomura, J. Tanaka, H. Miyatake, M. Fujioka, T. Shinozuka, M. Yoshii, H. Hama, K. Taguchi, K. Sueki, Y. Hatsukawa, K. Furuno and H. Kudo, *Nucl. Instr. and meth. B*26 (1987) 406.
- [25] A. Iivonen, R. Saintola and K. Valli, *Physica Scripta* 42 (1990) 133.
- [26] A. Iivonen, K. Riikonen, R. Saintola, K. Valli and K. Morita, *Nucl. Instr. and Meth. A*307 (1991) 69.
- [27] A. Iivonen, J. Kuhalainen, R. Saintola, K. Valli, T. Inamura, M. Koizumi, K. Morita and A. Yoshida, presented at the 12th international conference on electromagnetic

isotope separators and techniques related to their applications, and to be published in Nucl. Instr. and Meth.

- [28] S. Gerstenkorn and P. Luc, Atlas du Spectre D'Absorption de la Molècule D'Iode, (Centre National de la Recherche Scientifique, Paris, 1978).
- [29] M. Blann and H.K. Vonach, Phys. Rev. C28 (1983) 1475.
- [30] D.A. Eastham, P.M. Walker, J.R.H. Smith, J.A.R. Griffith, D.E. Evans, S.A. Wells, M.J. Fawcett and I.S. Grant, Optics Comm. 60 (1986) 293.
- [31] D.A. Eastham, P.M. Walker, J.R.H. Smith, D.D. Warner, J.A.R. Griffith, D.E. Evans, S.A. Wells, M.J. Fawcett and I.S. Grant, Phys. Rev. C36 (1987) 1583.
- [32] A. Werner and D. Zimmermann, Hyp. Int. 9 (1981) 197.
- [33] A. Kinbara, Sputtering-Gensyō (in Japanese), (Tokyo University Press, Tokyo, 1984).

公 表 論 文

- 1) Velocity distribution of ion beams from the RIKEN IGISOL
(理研 IGISOL からのイオンビームの速度分布)
M. Koizumi, Y. Yoshida, K. Morita, M. Takami, T.T. Inamura, M. Azuma, H. Katsuragawa, M. Nakaoka, I. Nakamura, T. Ishizuka, T. Murayama, A. Iivonen, K. Valli, K. Shimomura, S. Matsuki, and I. Sugai, to be published in Nucl. Instr. and Meth. (Dec. 1991).
- 2) Collinear fast atomic-beam laser spectroscopy at RIKEN GARIS/IGISOL
(理研 GARIS/IGISOL における共線高速原子線レーザー分光)
M. Koizumi, M. Azuma, T. Horiguchi, T.T. Inamura, T. Ishizuka, A. Iivonen, H. Katsuragawa, S. Matsuki, K. Morita, T. Murayama, I. Nakamura, M. Nakaoka, K. Shimomura, T. Shinozuka, I. Sugai, Y. Tagishi, M. Takami, K. Valli, M. Wakasugi, and A. Yoshida, presented at the Int. symposium on lasers in nuclear physics (Wako, 1991), and to be published in Hyp. Int.